Available online at www.sciencedirect.com

ScienceDirect

Geochimica et Cosmochimica Acta 257 (2019) 373–392

Geochimica et Cosmochimica Acta

www.elsevier.com/locate/gca

History of carbonate ion concentration over the last 100 million years II: Revised calculations and new data

Richard E. Zeebe [a,*], Toby Tyrrell [b]

[a] School of Ocean and Earth Science and Technology, University of Hawaii at Manoa, 1000 Pope Road, MSB 629, Honolulu, HI 96822, USA
[b] Ocean and Earth Science, University of Southampton, European Way, Southampton SO14 3ZH, UK

Received 26 September 2018; accepted in revised form 27 February 2019; available online 9 March 2019

Abstract

In an earlier contribution to this journal, we provided a reconstruction of seawater carbonate ion concentration over the last 100 million years (Tyrrell and Zeebe, 2004; TZ04 hereafter). Since then, multiple new and more robust data sets on past ocean carbonate chemistry, atmospheric CO_2, and major ion seawater composition have emerged, which prompt new CO_2 system reconstructions. In addition, we have gained new insight into the effects of past major ion seawater composition on equilibrium constants affecting CO_2 system calculations — most notably due to sulfate. Here we present new reconstructions of past ocean carbonate chemistry and atmospheric CO_2 based on new data and revised calculations, including error analysis. We also provide simple corrections for past equilibrium constants, supported by experimental data and well-suited for numerical models and observational studies on multi-million year time scales. Our updated result for just the seawater carbonate ion concentration (~2.3 to 4-fold lower 100 Myr ago) is similar to TZ04, indicating that our core approach is robust. However, all revised reconstructions using new alkenone and boron data now suggest that long-term ocean inventories of total dissolved inorganic carbon (DIC) and total alkalinity (TA) were similar to modern over the Cenozoic. This result contrasts strongly with one of TZ04's scenarios, which featured high Paleocene-Eocene DIC/TA inventories and was based on boron-derived *p*H values that have recently been revised. Because the carbonate system has two degrees of freedom, consistency checks can be made when three or more parameters are determined. Overall, our estimated long-term trends in CO_2 system parameters across the Cenozoic appear consistent, regardless of whether we combine our carbonate ion concentration with alkenone-derived pCO_2 or boron-derived *p*H. Our results suggest convergence towards a consistent picture of Cenozoic atmospheric CO_2 and seawater chemistry. Finally, we identify changes in past seawater sulfate as a conceptual and practical problem for seawater *p*H reconstructions.

Keywords: Carbon dioxide; Carbonate ion; Cenozoic; Seawater chemistry; pCO_2; Climate

1. INTRODUCTION

Reconstructing past atmospheric CO_2 concentrations and ocean carbonate chemistry is critical for understanding carbon cycle-climate feedbacks, climate sensitivity, ocean acidification and more (for recent reviews, see Kump et al., 2009; Hönisch et al., 2012; Zeebe, 2012a; Rohling et al., 2012). Tyrrell and Zeebe (2004) (TZ04) reconstructed the ocean's carbonate ion concentration ($[CO_3^{2-}]$) based on a simple but effective idea using the $CaCO_3$ saturation state (Ω) of seawater:

$$\Omega = \frac{[Ca^{2+}]\ [CO_3^{2-}]}{K^*_{sp}}, \quad (1)$$

where $[Ca^{2+}]$ is the dissolved calcium concentration and K^*_{sp} is the solubility product of calcite or aragonite; square

* Corresponding author.
E-mail addresses: zeebe@soest.hawaii.edu (R.E. Zeebe), Toby.Tyrrell@soton.ac.uk (T. Tyrrell).

https://doi.org/10.1016/j.gca.2019.02.041
0016-7037/

brackets denote stoichiometric concentrations. Briefly, given information on past $[Ca^{2+}]$, K^*_{sp}, and Ω, Eq. (1) can be solved for $[CO_3^{2-}]$ — an approach that has been widely cited and applied since (e.g., Locklair and Lerman, 2005; Pearson et al, 2009; Seki et al., 2010; Bartoli et al., 2011; Gillis and Coogan, 2011; Raven and Crawfurd, 2012; Boudreau and Luo, 2017; Sosdian et al., 2018). Prior to TZ04, attempts to reconstruct surface ocean carbonate chemistry considered calcite saturation as well but usually assumed constant seawater $[Ca^{2+}]$ in the past (e.g. Sundquist, 1986; Caldeira and Berner, 1999; Sundquist, 1999). TZ04 also pointed out that corrections for past equilibrium constants due to changes in major ion seawater composition are warranted, which has subsequently been considered in other applications, including numerical models (e.g., Zeebe et al., 2009; Ridgwell and Schmidt, 2010; Zeebe, 2012b).

Combining $[CO_3^{2-}]$ with a second carbonate chemistry parameter allows full CO_2 system reconstructions as two parameters are required to determine the system (plus temperature and salinity estimates) (e.g., Zeebe and Wolf-Gladrow, 2001). As the second parameter, TZ04 used GEOCARB pCO_2 (Berner and Kothavala, 2001) and a single δ^{11}B-based pH record available at the time (Pearson and Palmer, 2000), the latter of which has recently been revised (Anagnostou et al., 2016). Since then, multiple new and more robust data sets on past ocean carbonate chemistry, atmospheric CO_2, and major ion seawater composition have been published. This has prompted us to perform new CO_2 system reconstructions over the last 100 Myr, including error analysis. We also provide simple, updated corrections for past equilibrium constants that are supported by experimental data and can easily be used in numerical models and observational studies on multi-million year time scales.

2. PAST MAJOR ION SEAWATER COMPOSITION

As in TZ04, we use fluid inclusion data in this study to estimate past changes in major ion composition (Fig. 1a) (Horita et al., 2002; Lowenstein et al., 2003; Timofeeff et al., 2006; Brennan et al., 2013). While such estimates come with uncertainties (see original references for details), the general trends are consistent with other independent evidence for the seawater Mg/Ca ratio (Fig. 1b) such as the chemical compositions of calcifier fossils, inorganic calcite veins, etc. (see e.g., Stanley and Hardie, 1998; Dickson, 2002; Montañez, 2002; Tyrrell and Zeebe, 2004; Coggon et al., 2010; Evans and Müller, 2012; Rausch et al., 2013; Gothmann et al., 2015, and references therein). Our standard error envelopes (Fig. 1) assume zero errors at present (known modern values) and gradually increasing errors in the past. Note that given the long residence times of Ca^{2+} and Mg^{2+}, rapid swings that could be inferred from some of the data in Fig. 1a and b are implausible. For uncertainties in fluid inclusion reconstructions resulting from the value used for the product of $[Ca^{2+}] \times [SO_4^{2-}]$, see Section 5.3.2. Recent efforts to reconstruct seawater $[Ca^{2+}]$ based on foraminiferal Na/Ca ratios also yield trends

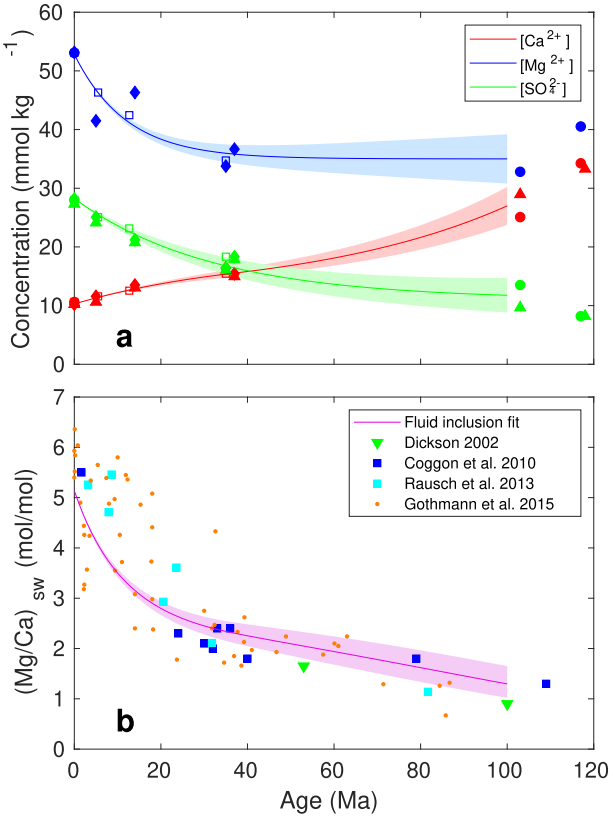

Fig. 1. (a) Past changes in $[Ca^{2+}]$, $[Mg^{2+}]$, and $[SO_4^{2-}]$ based on fluid inclusion data. Diamonds: Horita et al. (2002), triangles: Lowenstein et al. (2003), circles: Timofeeff et al. (2006), squares: Brennan et al. (2013). These studies assumed constant, modern $[Ca^{2+}] \times [SO_4^{2-}]$ over time to derive $[Ca^{2+}]$ and $[SO_4^{2-}]$ as shown, to which our estimated standard error envelopes apply (shaded areas). For errors from different $[Ca^{2+}] \times [SO_4^{2-}]$ values, see Section 5.3.2. Concentrations were converted from mmol kg^{-1}-H_2O to mmol kg^{-1}-solution using $S = 35$. Solid lines are exponential fits (standard fits hereafter) to obtain differentiable (smooth) curves over 100 Myr (see text). (b) Independent estimates of past seawater Mg/Ca ratios from echinoderms (Dickson, 2002), $CaCO_3$ veins (Coggon et al., 2010; Rausch et al., 2013), and fossil corals (Gothmann et al., 2015). The purple line and envelope show seawater Mg/Ca and propagated errors from fit to fluid inclusions in (a). Standard envelopes assume zero errors at present (known modern values) and gradually increasing errors in the past. Given the long residence times of Ca^{2+} and Mg^{2+}, rapid swings that might be inferred from some of the data in (a) and (b) are implausible. (For interpretation of the references to colour in this figure legend, the reader is referred to the web version of this article.)

broadly consistent with those from fluid inclusions (Hauzer et al., 2018; Zhou et al., 2018).

Past major ion changes (Fig. 1) have important implications for our reconstructions. First, given Eq. (1), one key consequence of higher $[Ca^{2+}]$ in the past (Fig. 1) is that $[CO_3^{2-}]$ must have been lower (everything else being equal). It turns out that this overriding consideration dominates despite past changes in Ω and K^*_{sp} (see Sections 4 and 5). The two- to threefold decline in $[Ca^{2+}]$ over the past 100 Ma forced a compensating large increase in $[CO_3^{2-}]$.

Second, chemical equilibrium constants (K^*'s) used to calculate ocean carbonate chemistry depend on the major constituents of seawater, which have varied in the past. Hence K^*'s require corrections over time, which we provide below (see Section 3).

Exponential functions were fit over 100 Myr to the estimated concentrations from fluid inclusions for $[Ca^{2+}]$, $[Mg^{2+}]$, and $[SO_4^{2-}]$; x_j's for short, where $j = 1, 2, 3$ (see Fig. 1a, Table 1):

$$x(t) = (x' - x'')\, e^{-(t-t_1)/\tau} + x'', \tag{2}$$

where x', x'', t_1, and τ are constants (see Table 1). Note that there is no mechanistic reason for an exponential fit. In fact, between 37 and 100 Ma, the fit is unconstrained and one could select a linear fit as the parsimonious model. We only use exponentials here to obtain differentiable (smooth) curves over 100 Myr. Below, we will discuss flux estimates based on derivatives, which would produce artificial flux spikes for non-smooth curves.

One critical requirement for past reconstructions of seawater chemistry is that charge balance must be maintained. That is, the sum of all positive charges must equal the sum of all negative charges at all times. It turns out that the estimated changes in x_j's alone (standard fits, Fig. 1a) would produce a charge imbalance of up to +30 mmol kg^{-1} in the past (the $[SO_4^{2-}]$ decline remains essentially unbalanced), although the magnitude of the imbalance depends on the product of $[Ca^{2+}] \times [SO_4^{2-}]$ assumed in the fluid inclusion studies, see Section 5.3.2. If correct, the imbalance is significant and was unlikely compensated for by minor constituents. Rather, other major ions would have to make up for the imbalance such as Cl^-, Na^+, and K^+. Cl^- has a very long residence time and $[K^+]$ probably changed very little over the Phanerozoic (Horita et al., 2002). This leaves changes in $[Na^+]$ to maintain charge balance. In fact, this assumption has been made to reconstruct $[Na^+]$ in the past (e.g., Timofeeff et al., 2006; Brennan et al., 2013). If the same assumption is made here, it would lead to ~30 mmol kg^{-1} lower $[Na^+]$ at 100 Ma for the standard scenario (Fig. 2). Do such changes in Na^+ inventory and flux appear feasible, given sodium's residence time in the ocean?

The change in Na^+ influx (ϕ) required to produce the estimated past change in the ocean's $[Na^+]$ inventory (Fig. 2) may be estimated from:

$$\frac{dM_{Na^+}}{dt} = \phi - (1/\tau_{Na^+}) \cdot M_{Na^+}, \tag{3}$$

Table 1
Fit parameters for Eq. (2).

		x'	x''	t_1	τ
Ca^{2+}	[a]	10.280	19.000	0	40.000
Ca^{2+}	[b]	15.542	11.478	37	−47.011
Mg^{2+}	[c]	52.820	35.000	0	12.000
SO_4^{2-}	[c]	28.240	11.000	0	32.000

[a] $t = [0\ 37]$.
[b] $t = [37\ 100]$.
[c] $t = [0\ 100]$ Ma.

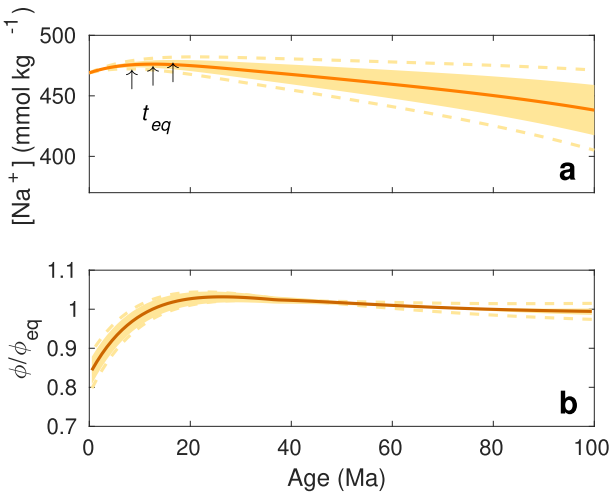

Fig. 2. (a) Past seawater $[Na^+]$ derived from fits to fluid inclusion data (Fig. 1a) and charge balance (see text). The envelope represents standard errors propagated from Fig. 1a. Dashed lines estimate errors due to different $[Ca^{2+}] \times [SO_4^{2-}]$ values by doubling the standard errors for $[Ca^{2+}]$ and $[SO_4^{2-}]$, see Section 5.3.2. (b) Inferred Na^+ influx based on Eq. (3). Note that the steady-state flux (ϕ_{eq}) corresponds to time t_{eq} where $[Na^+]$ is at maximum ($d[Na^+]/dt = 0$), not to $t = 0$. The ratio $\phi/\phi_{eq} = 1$ occurs at t_{eq}, which varies for each scenario (arrows) and in turn give different flux estimates at $t = 0$.

where M_{Na^+} is the Na^+ inventory and τ_{Na^+} is the residence time of Na^+. Given M_{Na^+} over time (Fig. 2), its derivative can be calculated. Using $\tau_{Na^+} \simeq 50$ Myr (Berner and Berner, 2012; Lécuyer, 2016), Eq. (3) can then be solved for ϕ. As a result, the Na^+ influx would have to change by less than ~20% over the past 100 Myr to explain the seawater Na^+ concentrations as implied by fluid inclusions (Fig. 2). However, note that these estimates have large uncertainties beyond those suggested by the error envelopes, including intrinsic errors in individual fluid inclusion reconstructions (e.g., Section 5.3.2), assumptions about constant $[Cl^-]$ and $[K^+]$, Na^+ residence time, neglecting changes in minor constituents, etc. Note also that it is not clear what would have caused the relatively rapid decrease in Na^+ flux over the past 10–15 Myr (Fig. 2). Finally, changes in $[Na^+]$ of the indicated magnitude have a small effect on our overall results. For example, calculated sensitivity parameters for past K^* corrections (see Section 3.2) show modest changes with $[Na^+]$ (Tables 2 and D.1) and our carbonate chemistry reconstructions are not overly sensitive to changes in K^*'s (see Section 5.3).

2.1. Artificial paleo-seawater

Regardless of uncertainties in past major ion changes, it may be desirable to prepare artificial seawater with major ion composition different from modern, e.g., for geochemical or biological purposes (e.g., Mucci and Morse, 1984; Ries, 2004; Haynes et al., 2017; Zeebe and Tyrrell, 2018). If such artificial seawater were to resemble major ion changes as discussed here, including $[Ca^{2+}]$, $[Mg^{2+}]$, and

$[SO_4^{2-}]$, one option is to vary the salt concentrations of NaCl, $CaCl_2$, $MgCl_2$, and Na_2SO_4. However, note that this is only one option and does not necessarily reflect actual paleo-seawater changes.

If the goal is, for instance, to maintain charge balance by adjusting $[Na^+]$ at constant $[Cl^-]$, then mole-by-mole differences in salt additions/reductions (Δ's) may be obtained from $\Delta NaCl = n\Delta MA_2$, where M = Ca or Mg, A = Cl, and $n = -2$. That is, for example, a rise in $[Ca^{2+}]$ by x (in appropriate units) is compensated for by a $2x$-drop in $[Na^+]$. Changes in $[SO_4^{2-}]$ may be achieved by simply adjusting the amount of Na_2SO_4 added. If the goal is to maintain constant ionic strength (I) by adjusting NaCl, then $n = -3$ for the above recipe; furthermore $\Delta NaCl = n\Delta Na_2SO_4$. The factor 3 arises from the fact that the ions of the salt with one doubly charged ion (say MA_2 or Na_2SO_4) contribute 3 units to $\Delta I = \sum z_i^2 x_i/2 = (2^2x + 1^2 \cdot 2x)/2 = 3x$, whereas NaCl contributes only one unit: $(1^2x + 1^2x)/2 = 1x$. For this constant ionic strength scenario, of course both total $[Na^+]$ and $[Cl^-]$ change, with their net change being given by the sum of the individual additions/reductions of the salts that contain them. For example, raising $[SO_4^{2-}]$ by x via Na_2SO_4 addition requires NaCl reduction by $3x$, hence a net $[Na^+]$ change by $2x - 3x = -x$. The charge balance and constant ionic strength scenarios appear relevant to a variety of problems and have been applied in chemical and physiological studies. Indeed, charge and ionic strength are likely critical for a variety of geochemical and biological processes given their nature of ionic interactions, rather than, for instance, total salt content (mass). We will therefore provide corrections for stoichiometric equilibrium constants for the charge balance and constant ionic strength scenarios below (Section 3.2, Appendix D).

3. EFFECTS OF $[CA^{2+}]$, $[MG^{2+}]$, AND $[SO_4^{2-}]$ ON STOICHIOMETRIC EQUILIBRIUM CONSTANTS

As detailed in Section 2, there is compelling evidence for large changes in major ion seawater composition over the last 100 Myr. Among the major ions, changes in $[Ca^{2+}]$, $[Mg^{2+}]$, and $[SO_4^{2-}]$ are most critical for our carbonate chemistry reconstructions through their effect on $[CO_3^{2-}]$ (for $[Ca^{2+}]$, see Eq. (1)) and stoichiometric equilibrium constants. The concentrations of Na^+, Cl^-, and K^+ appear to have varied only slightly over the last 100 Myr (see Section 2). In Appendix B, we examine the effects of changes in $[Ca^{2+}]$, $[Mg^{2+}]$, and $[SO_4^{2-}]$ on the dissociation constants of carbonic acid (K_1^* and K_2^*) and calcite solubility (K_{spc}^*). We restrict our discussion to these constants for three reasons. First, K_1^*, K_2^*, and K_{spc}^* are by far the most important constants entering our calculations. Second, the effect of changes in the remaining constants (e.g., $K_0, K_w, \ldots$) are dwarfed by uncertainties in other parameters, including the reconstruction of the major ion seawater composition itself. Third, it turns out that our results are not overly sensitive to changes in K^*'s (see Section 5.3).

We compare all inferred major effects of $[Ca^{2+}]$, $[Mg^{2+}]$, and $[SO_4^{2-}]$ on K_1^*, K_2^*, and K_{spc}^* to actual experimental data when deriving our K^* corrections. Reviewing the experimental data requires some work (Appendix B) but provides the only rigorous check on chemical seawater models (see note below). Given the various uncertainties and limited available experimental data, we focus on data at 25 °C to derive corrections for the K^*'s.

In this paper, we denote thermodynamic and stoichiometric constants by K and K^*, respectively. Curly and square brackets denote activities (also a_i's) and stoichiometric concentrations, respectively. The equilibrium constants for the dissociation of carbonic acid and calcite solubility may be written as:

$$K_1 = \frac{\{HCO_3^-\}\{H^+\}}{\{CO_2\}a_{H_2O}}; \quad K_1^* = \frac{[HCO_3^-][H^+]}{[CO_2]} \tag{4}$$

$$K_2 = \frac{\{CO_3^{2-}\}\{H^+\}}{\{HCO_3^-\}}; \quad K_2^* = \frac{[CO_3^{2-}][H^+]}{[HCO_3^-]} \tag{5}$$

$$K_{spc} = \{Ca^{2+}\}_{sat}\{CO_3^{2-}\}_{sat}; \quad K_{spc}^* = [Ca^{2+}]_{sat}[CO_3^{2-}]_{sat}, \tag{6}$$

where 'sat' signifies saturation; for a_{H_2O}, see Appendix A. Introducing the total activity coefficient γ_i of species i, with $\{i\} = \gamma_i\,[i]$, we can express the stoichiometric constants by total activity coefficients and thermodynamic K's, which are constants at given temperature and pressure (i.e., do not depend on salinity, composition, etc.):

$$K_1^* = K_1 \frac{\gamma_{CO_2}}{\gamma_{HCO_3^-}\gamma_{H^+}}\, a_{H_2O} \tag{7}$$

$$K_2^* = K_2 \frac{\gamma_{HCO_3^-}}{\gamma_{CO_3^{2-}}\gamma_{H^+}} \tag{8}$$

$$K_{spc}^* = K_{spc} \frac{1}{\gamma_{Ca^{2+}}\gamma_{CO_3^{2-}}}; \tag{9}$$

for γ_{CO_2}, see Appendix A. The above relationships are useful when illustrating the effects of different major ion concentrations on stoichiometric equilibrium constants (Appendix B). Furthermore, for the free activity coefficient we have $\{i\} = \gamma_i^F\,[i]_F$, and hence $\gamma_i/\gamma_i^F = [i]_F/[i]$, where $[i]$ is the total concentration (free + complexed). Note that the K's and K^*'s in Eqs. (7)–(9) should be expressed in the same units. For example, K's and K^*'s are often reported in units of mol kg^{-1}-H_2O (molality, concentration symbol m_i) or mol kg^{-1}-solution (molamity, see Ramette, 2004), respectively. The conversion factor from molality to molamity at standard seawater composition is $w2s \simeq 1 - (0.001005 \times S)$, where S is salinity (e.g., Millero, 1995).

3.1. Note on chemical models for seawater

For the present study, Millero and Schreiber's (1982) chemical model for seawater (MS82 hereafter) turned out to be helpful (see Appendix B). The model is based on the idea of ion pairing and builds on the work of Garrels and Thompson (1962) and others. However, we emphasize that we do not advocate here the universal use of ion-pairing models over, say, Pitzer models (though cf. Zeebe

and Tyrrell, 2018) or other theoretical approaches and do not argue for or against the theoretical basis of one particular model (cf. May and Rowland, 2017). In this context, it is noteworthy that Pitzer models for seawater actually include explicit ion pairing for some dissolved species and that more recent work on ion pairing in the carbonic acid system (e.g. Stefánsson et al., 2013, 2014, 2017) is largely consistent with earlier work that formed the basis for various parameters used in Millero and Schreiber (1982).

Nevertheless, chemical models for seawater still have large uncertainties and the data on which they are based are in some cases insufficient, inconsistent, or lacking altogether (discussed in Appendix B). To improve the situation for studies such as the present one, we advocate the experimental determination of stoichiometric equilibrium constants for the particular major ion compositions of past oceans, i.e., at minimum including variations of the concentrations of Ca^{2+}, Mg^{2+}, and SO_4^{2-} over relevant ranges (e.g., Horita et al., 2002). The currently available data for K_1^*, K_2^*, and K_{spc}^* are examined in Appendix B.

3.2. Summary: equilibrium constants

As described in Appendix B, the trends expected from Eqs. (7)–(9) for the effects of calcium, magnesium, and sulfate on stoichiometric equilibrium constants and activity coefficients are consistent with data from various laboratory measurements. Also, for the present purpose, the trends predicted by the ion-pairing model (IPM, based on Millero and Schreiber, 1982) are sufficiently close to the observed trends (Figs. B.1–B.3, B.5). Importantly, absolute values predicted by the IPM are secondary for our approach. As in Tyrrell and Zeebe (2004), we use established standard stoichiometric K^*'s below (experimentally determined using modern seawater media as standard states) and only apply relative changes to K^*'s as functions of $[Ca^{2+}]$, $[Mg^{2+}]$, and $[SO_4^{2-}]$ (x_j's for short, where $j = 1, 2, 3$). In the following, we will use the IPM trends to correct K^*'s for past changes in seawater composition. Our calculations also include changes in $[Na^+]$ and I, which affects free activity coefficients of ionic species, γ_{CO_2}, a_{H_2O}, etc. (see Appendix A).

For relevant ranges of x_j changes in the past (see Section 2), the relative changes in K^*'s (or K^* ratios) predicted by the IPM are virtually linear when x_j's vary individually (Fig. 3). Even when x_j's vary simultaneously, K^* ratios remain very close to linear (see Appendix C), allowing a simple linear parameterization to a very good approximation (Ben-Yaakov and Goldhaber, 1973; Tyrrell and Zeebe, 2004), although with new sensitivity parameters s_{ij}:

$$K_i^*/K_{i,m}^* = 1 + \sum_{j=1}^{3} s_{ij}\,\left(x_j/x_{j,m} - 1\right) \qquad (10)$$

where $m = \text{modern}, i = 1, 2, \text{spc}$, and x_j refers to $[Ca^{2+}]$, $[Mg^{2+}]$, and $[SO_4^{2-}]$. The s_{ij} were obtained from linear fits to the IPM results shown in Fig. 3 for maintaining charge balance via $[Na^+]$ adjustment (see Table 2). Parameters for constant ionic strength are given in Appendix D. The computational effort for our approach is minimal and well-suited for easy K^*-corrections in numerical models as well as observational studies, at an accuracy appropriate for seawater carbonate chemistry and CO_2 reconstructions on multi-million year time scales.

Table 2
Sensitivity parameters $s_{ij} \times 10^3$ (dimensionless) for Eq. (10) with $[Na^+]$ adjustment to maintain charge balance.

	K_1^*	K_2^*	K_{spc}^*
Ca^{2+}	5	157	185
Mg^{2+}	17	420	518
SO_4^{2-}	208	176	106

Given past changes in major ion composition (Fig. 1a) and the effects of $[Ca^{2+}]$, $[Mg^{2+}]$, and $[SO_4^{2-}]$ on K^*'s as estimated above (Fig. 3), corrections for past stoichiometric equilibrium constants can then be calculated (Eq. (10), Fig. 4). These K^* ratios will be used below to calculate carbonate chemistry parameters over time.

4. LONG-TERM TRENDS IN OCEAN CARBONATE CHEMISTRY OVER THE LAST 100 MYR

From the history of $[Ca^{2+}]$ (Fig. 1a) and seawater calcite saturation state (Tyrrell and Zeebe, 2004), we estimate the long-term evolution of surface $[CO_3^{2-}]$ over the last 100 Myr (Fig. 5a). It turns out that our new surface $[CO_3^{2-}]$ is very similar to that published 14 years ago (Tyrrell and Zeebe, 2004), except being slightly higher at 100 Ma. The reason for the similarity is that changes due to updates in equilibrium constants (raising past $[CO_3^{2-}]$) are partly compensated for by higher reconstructed $[Ca^{2+}]$ (lowering past $[CO_3^{2-}]$). Combining $[CO_3^{2-}]$ with one other carbonate chemistry parameter (plus T, S estimates) allows computation of the remaining carbonate chemistry parameters.

We emphasize that our reconstructions based on $[CO_3^{2-}]$ are inherently long-term trend estimates over $\gtrsim$ 10-Myr intervals. We do not resolve events and aberrations such as the MECO, the hyperthermals (PETM, ELMO, ...), etc. Likewise, changes in trends on time scales $\lesssim$ 10 Myr are not resolved, including those during the early Paleogene, which warrant a more detailed analysis (e.g., Komar et al., 2013). One exception is the Middle Miocene Climatic Optimum (MMCO, ~17–15 Ma), which we briefly discuss below in the context of boron isotope data.

4.1. Long-term trends from $[CO_3^{2-}]$ and atmospheric CO_2

In this section we use independent pCO_2 estimates either from GEOCARB modeling or from alkenones as the second parameter (Fig. 5). Estimates for T and S used for the GEOCARB scenario were unchanged from Tyrrell and Zeebe (2004), while T information for the alkenone scenario were directly taken from each of the published alkenone data sets without smoothing; S was assumed constant (cf. also www.p-co2.org and Rae (2018)). The modern surface $[CO_3^{2-}]$ was set to 200 μmol kg^{-1} for the GEOCARB scenario, corresponding to preindustrial values of $pCO_2 = 280$ μatm and $pH = 8.18$ on the total scale

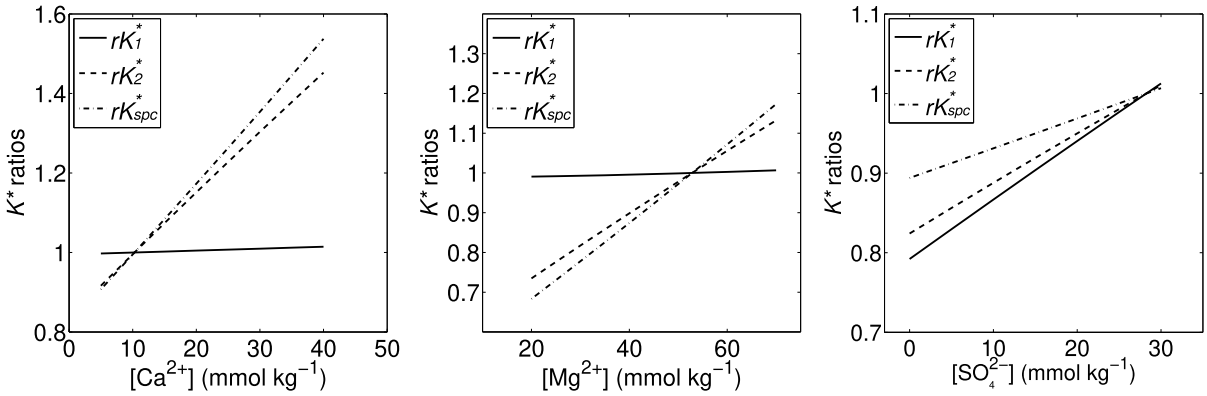

Fig. 3. Changes in K^* ratios relative to modern ($rK^* = K^*/K^*_m$) predicted by the ion-paring model (IPM) based on Millero and Schreiber (1982). Results are for standard seawater composition, except for changes in $[Ca^{2+}]$, $[Mg^{2+}]$, and $[SO_4^{2-}]$ as shown and in $[Na^+]$ to maintain charge balance. Calculations also include changes in I, which affects free γ's of ions, γ_{CO_2}, a_{H_2O}, etc. (see Appendix A).

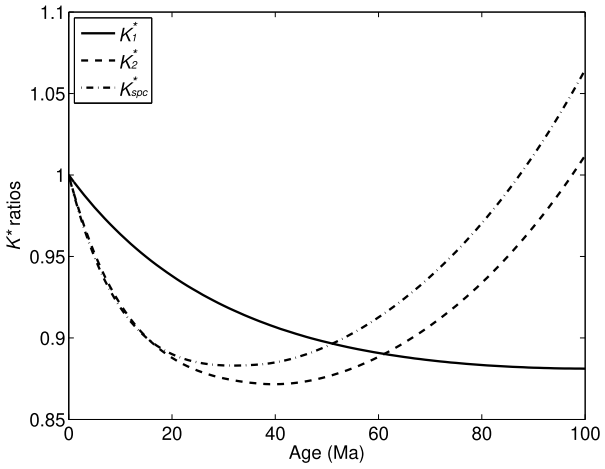

Fig. 4. Past changes in K^*'s (or K^* ratios, Eq. (10)) estimated from reconstructed changes in $[Ca^{2+}]$, $[Mg^{2+}]$, and $[SO_4^{2-}]$ (Fig. 1a) and effects on K^*'s (Fig. 3). $[Na^+]$ was adjusted to maintain charge balance.

(Zeebe and Wolf-Gladrow, 2001) at a global mean sea surface temperature of $T \simeq 15\,^{\circ}C$. For the alkenone scenario, modern surface $[CO_3^{2-}]$ was set to 250 μmol kg^{-1}, more representative for modern sea surface temperatures of $T \gtrsim 20\,^{\circ}C$ at the latitudinal site distribution of the alkenone studies included here (Fig. 5a).

Using our $[CO_3^{2-}]$ and the pCO_2 reconstructions, surface ocean DIC (total dissolved inorganic carbon), TA (total alkalinity), and pH can be calculated (Fig. 5). At present, no independent reliable proxies exist for DIC and TA. However, we can use surface ocean pH estimates from stable boron isotope records ($\delta^{11}B$) as an independent check on the $[CO_3^{2-}] + pCO_2$ combination (Fig. 5e). Again, note that the GEOCARB time step is of order 10 Myr and hence does not resolve events (MECO, PETM, ELMO, etc.) and changes in trends $\lesssim 10$ Myr, say, during the early Paleogene (e.g., Komar et al., 2013). Overall, the trends in CO_2 system parameters across the Cenozoic appear consistent. For example, consistency for pH may be quantified by calculating the difference (ΔpH) between pH values derived from the $[CO_3^{2-}]$ + alkenone pCO_2 combination vs. pH values derived from boron (Fig. 5e). Using a series of 1-Myr bins in which the two data sets overlap ($N = 16$), the average absolute ΔpH over the last 45 Myr is ~0.07 pH units (much larger, i.e., ~0.12 pH units if we assumed constant, modern $[CO_3^{2-}]$). For comparison, the reported errors on boron-based pH for records younger than ~20 Ma, are typically 0.02–0.07 units (Seki et al., 2010; Bartoli et al., 2011; Martínez-Botí et al., 2015) and 0.05–0.07 units for the Eocene records (Pearson et al, 2009; Anagnostou et al., 2016) but can be larger if uncertainties in seawater $\delta^{11}B$ are fully propagated. Importantly, however, ΔpH can be caused not only by errors but also by natural short-term and/or spatial environmental variability, e.g., when combination-pH and/or boron-pH values are not from exactly the same times or cores. To illustrate this point, we have also calculated the average standard deviation ($\overline{\sigma}$) of independent boron-pH values in the same 1-Myr bin, for bins containing more than one value ($N = 12$), which yields $\overline{\sigma} \simeq 0.04$ pH units.

Pagani et al. (2011) and Zhang et al. (2013) both reported one rather high alkenone-pCO_2 value >2500 μatm at ~36 Ma (Fig. 5b) from the same core interval at ODP Site 925, only Zhang et al. used a different age model and parameters to calculate pCO_2. Hence, only one value should be displayed in compilations, not both. The reason for the unusually high value remains unclear but is unlikely to be a measurement error.

When comparing CO_2 system parameters, one needs to be careful in selecting truly independent variables to avoid circularity. For example, the pCO_2 obtained from $\delta^{11}B$ records is a derived variable because it is based on pH, which requires one additional parameter and is therefore not an independent quantity in the context of carbonate chemistry. In fact, most boron-based studies make assumptions about past DIC, TA, or $[CO_3^{2-}]$ to derive pCO_2. Hence if one were to use $\delta^{11}B$-derived pCO_2 as the second parameter, one would essentially recover DIC, TA, or $[CO_3^{2-}]$ values as assumed in the first place, which is circular. However, we may use our $[CO_3^{2-}]$ plus $\delta^{11}B$-pH to derive pCO_2 and

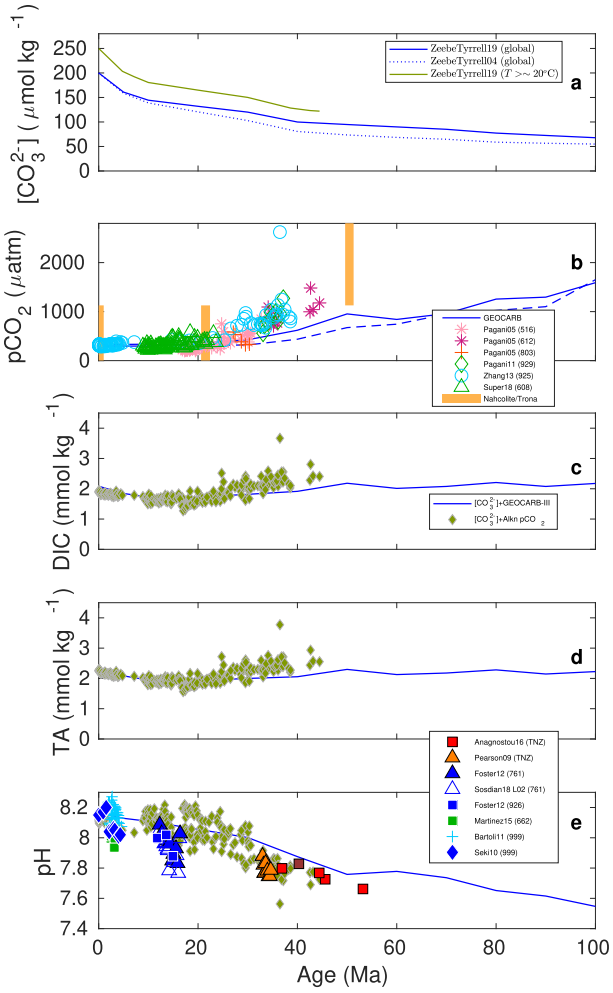

Fig. 5. Estimates of carbonate chemistry parameters from (a) surface ocean $[CO_3^{2-}]$ (this study & TZ04) and (b) pCO_2. Independent pCO_2 estimates are from GEOCARB-III and GEOCARB-SULF (dashed) (Berner and Kothavala, 2001; Berner, 2006, 2008) and alkenones (e.g., Pagani et al., 2005, 2011; Zhang et al., 2013; Super et al., 2018). Bars: ranges from mineral-phase equilibria (Nahcolite/Trona) (Lowenstein, 2006). The GEOCARB and alkenone scenarios use $[CO_3^{2-}]$ corresponding to global modern mean $T \simeq 15\,^{\circ}C$ and $T \gtrsim 20\,^{\circ}C$ (see (a)). The results for pH (blue line, olive diamonds in (e)) may be compared to independent boron-based pH estimates (see legend) (e.g., Pearson et al, 2009; Seki et al., 2010; Bartoli et al., 2011; Foster et al., 2012; Martínez-Botí et al., 2015; Anagnostou et al., 2016; Sosdian et al., 2018), cf. also www.p-co2.org and Rae (2018). Our results are available at www.soest.hawaii.edu/oceanography/faculty/zeebe_files/ZT19.html. (For interpretation of the references to colour in this figure legend, the reader is referred to the web version of this article.)

compare our results to independent pCO_2 estimates (Section 4.2).

4.2. Long-term trends from $[CO_3^{2-}]$ and pH

In this section we use our $[CO_3^{2-}]$ together with independent pH estimates from $\delta^{11}B$ records as the second parameter (Fig. 6). Temperature estimates for the pH scenarios were taken from the published $\delta^{11}B$ data sets. For the pH scenario, modern surface $[CO_3^{2-}]$ was set to 280 µmol kg^{-1}, more representative for modern sea surface temperatures of $T \gtrsim 25\,^{\circ}C$ at the latitudinal site distribution of the boron studies included here (Fig. 6a). As explained in Section 3, compared to the effects of seawater composition on K_1^*, K_2^*, K_{sp}^*, and various other uncertainties, effects of changes in the boric acid dissociation constant K_B^* are small. Moreover, for our parameter combinations, K_B^* only affects TA estimates. For instance, changing K_B^* by 20%, yields $\Delta TA \simeq 10$ µmol kg^{-1}. The Cenozoic long-term evolution of boron-derived pH appears consistent with pH from our $[CO_3^{2-}]$ and GEOCARB pCO_2 (dashed line, Fig. 6b),

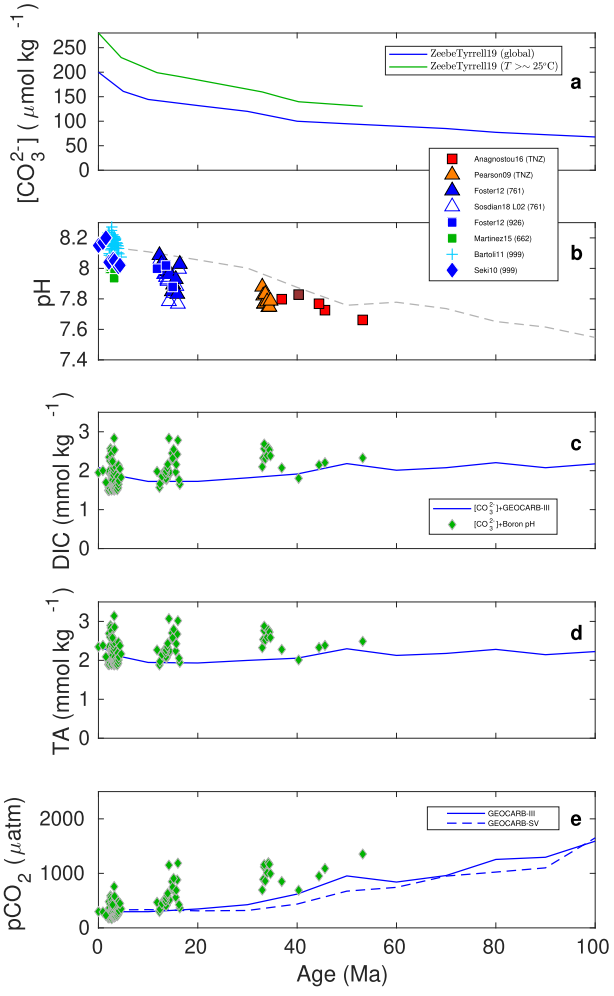

Fig. 6. Estimates of carbonate chemistry parameters from (a) surface ocean $[CO_3^{2-}]$ (this study) and (b) independent pH estimates from boron-based studies (symbols, cf. also www.p-co2.org and Rae (2018)). The pH scenarios use surface $[CO_3^{2-}]$ corresponding to $T \gtrsim 25\,^{\circ}C$ (see (a)). In (e), GEOCARB-SV: GEOCARBSULF model including volcanic rock weathering. For references, see Fig. 5. Dashed line in (b) shows pH from our $[CO_3^{2-}]$ and GEOCARB-pCO_2 for comparison. Our results are available at www.soest.hawaii.edu/oceanography/faculty/zeebe_files/ZT19.html.

although boron-pH is generally lower in the past, particularly during intervals such as the Middle Miocene Climatic Optimum (MMCO, ~17–15 Ma) and the Eocene-Oligocene Transition (EOT), which are not resolved in GEOCARB. Correspondingly, pCO$_2$ derived from our [CO_3^{2-}] and δ^{11}B-pH is generally higher than the GEOCARB estimates (Fig. 6e).

However, note that our reconstructions for intervals such as the MMCO should be taken with caution because they combine one inherent long-term (our [CO_3^{2-}]) and one short-term parameter (boron-pH) during relatively fast Earth system changes. Short-term variations in [CO_3^{2-}] during the MMCO are of course possible, if not likely, and because they are not resolved, bias our reconstructions (potentially overestimating pCO$_2$ for the low-pH data). Also note that Sosdian et al. (2018) provided various additional pH scenarios for ODP Site 761 (cf. Foster et al., 2012). Thus we have included one "high-pH" MMCO scenario (Foster et al., 2012) and one of the "low-pH" scenario, labeled "Sosdian18 L02" (Figs. 5e and 6b), which uses Lemarchand et al. (2002)'s seawater δ^{11}B (Sosdian et al., 2018).

5. DISCUSSION

5.1. Past DIC and TA inventories

Our reconstructions suggest that long-term DIC and TA were similar to modern values across the past 100 Myr, regardless of whether pCO$_2$ or pH is used as the second parameter with our [CO_3^{2-}] (Figs. 5 and 6). This may appear surprising, given that Cenozoic pCO$_2$ was mostly higher than modern, which, everything else being the same, would suggest elevated DIC (see Zeebe and Wolf-Gladrow, 2001). However, the relatively low DIC despite high pCO$_2$ is a direct consequence of higher [Ca^{2+}] in the past, which leads to lower [CO_3^{2-}], given moderate changes in carbonate saturation (Fig. 5a). Briefly, the effect of elevated past CO$_2$ levels on DIC was largely compensated for by lower [CO_3^{2-}].

5.2. CCD records

As discussed in detail in TZ04, records of the calcite compensation depth (CCD) indicate that the ocean's calcite saturation state (Ω) has not varied dramatically over the past 100 Myr. Nevertheless, to account for changes in whole-ocean saturation, TZ04 used a smoothed global CCD curve (Fig. 7), which should reflect changes in Ω. In turn, changes in Ω affect [CO_3^{2-}] via Eq. (1) (see Appendix E), but to what extent? The effect of CCD changes on our calculated [CO_3^{2-}] may be illustrated by replacing the global CCD curve by reconstructions for the equatorial Pacific CCD (Pälike et al., 2012). This test merely serves as an illustration; we emphasize that the equatorial Pacific CCD is not a substitute for the global CCD. Nevertheless, the effect is small (Fig. 7), suggesting that our [CO_3^{2-}] reconstruction is insensitive to details of Ω/CCD changes across the Cenozoic.

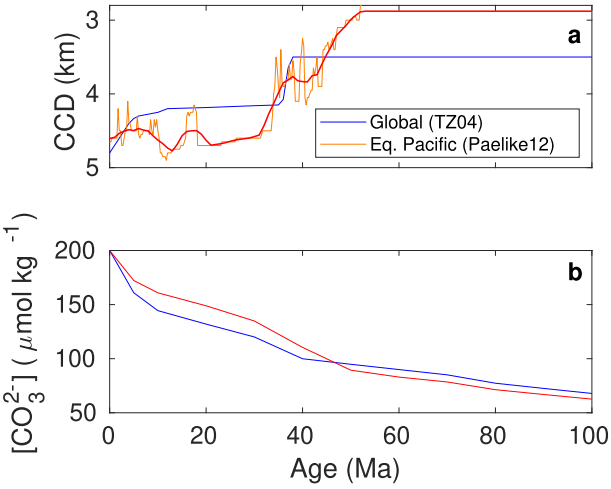

Fig. 7. Effect of (a) calcite compensation depth (CCD) on (b) [CO_3^{2-}] via saturation state Ω (see text). Default calculations use changes in global CCD after TZ04 (blue lines). Red lines illustrate the effect on [CO_3^{2-}] if reconstructions for the equatorial Pacific CCD were used instead (Pälike et al., 2012). We emphasize, however, that the equatorial Pacific CCD is not a substitute for the global CCD. Because our [CO_3^{2-}] proxy is inherently long-term (see text), a smoothed curve (thick red line in (a)) was used. To allow comparison with the global CCD record (blue curve in (a)), the red curve was set constant between 50 and 100 Ma. (For interpretation of the references to colour in this figure legend, the reader is referred to the web version of this article.)

5.3. Error propagation

Uncertainties in our reconstructions may be evaluated by assigning errors to important parameters and propagating those through the calculations. Important parameters that affect our results include changes in temperature (T), salinity (S), major ion concentrations, sensitivity parameters for K^* corrections (s_{ij}), and the ocean's calcite saturation state (Ω), as inferred from CCD changes. Additional parameters enter the calculations but not all are critical. For instance, the total boron concentration in seawater makes no difference for pH, when calculated from [CO_3^{2-}] and [CO_2], although it does affect TA (Zeebe and Wolf-Gladrow, 2001). In the following, we focus on the parameters listed above, which are most critical for our reconstructed pH and pCO$_2$. Importantly, our error propagation provides uncertainty estimates for our results based on given, assigned parameter errors. The assigned errors themselves are somewhat arbitrary and mostly chosen rather generously. For example, an assigned maximum temperature error of ±5 K at 100 Ma (see below) is most likely at the upper end of realistic values. Hence our emphasis is on providing what-if scenarios, rather than precise parameter errors.

5.3.1. Individual error propagation

To illustrate the effect of uncertainties in individual parameters on our results, in this section we propagate errors separately for two scenarios. First, we calculate pH from our [CO_3^{2-}] (including errors) and GEOCARB pCO$_2$

(Fig. 8, middle column). Second, we calculate pCO_2 from our $[CO_3^{2-}]$ (including errors) and the standard pH result of the first (GEOCARB) scenario (Fig. 8, right column). This allows for easy inspection of pH and pCO_2 uncertainties for related scenarios. The emphasis here is on estimating maximum uncertainties from individual parameters and will involve some non-standard assumptions about errors.

Errors in T, S, and CCD were assumed to grow linearly with time in the past so that the maximum error was assigned at 100 Ma (variables with subscript label '100' in Fig. 8). T and S affect the various equilibrium constants, with an opposite net effect on our calculated pCO_2. Hence we combined an increase in T with a drop in S and vice versa (Fig. 8, 1st row). The major ion concentrations ($[Ca^{2+}]$, $[Mg^{2+}]$, $[SO_4^{2-}]$) were varied within their estimated standard error envelopes (see Fig. 1a); for uncertainties resulting from the value used for $[Ca^{2+}] \times [SO_4^{2-}]$, see Section 5.3.2. Sensitivity parameters for K^* corrections (s_{ij}) were assigned a constant error of ±100%, while Ω was varied corresponding to an assigned maximum CCD error of ±1 km at 100 Ma.

The propagated uncertainty for $[CO_3^{2-}]$ and pH is moderate; for pCO_2 it is more significant (ca. ±300 µatm). However, note that the assigned maximum parameter errors at 100 Ma of $T \pm 5$ K and $S \mp 3$ are rather large. Varying $[Ca^{2+}]$, $[Mg^{2+}]$, and $[SO_4^{2-}]$ within their estimated error envelopes (Fig. 1a) has a small effect on $[CO_3^{2-}]$ and pH, and a slightly larger impact on pCO_2, ca. ±250 µatm (Fig. 8, 2nd row). Large changes in sensitivity parameters s_{ij} for K^* corrections by ±100% (factor 0 and 2) only have a moderate effect throughout (Fig. 8, 3rd row). As a result, using no corrections at all ($0 \times s_{ij}$ means modern K^*'s)

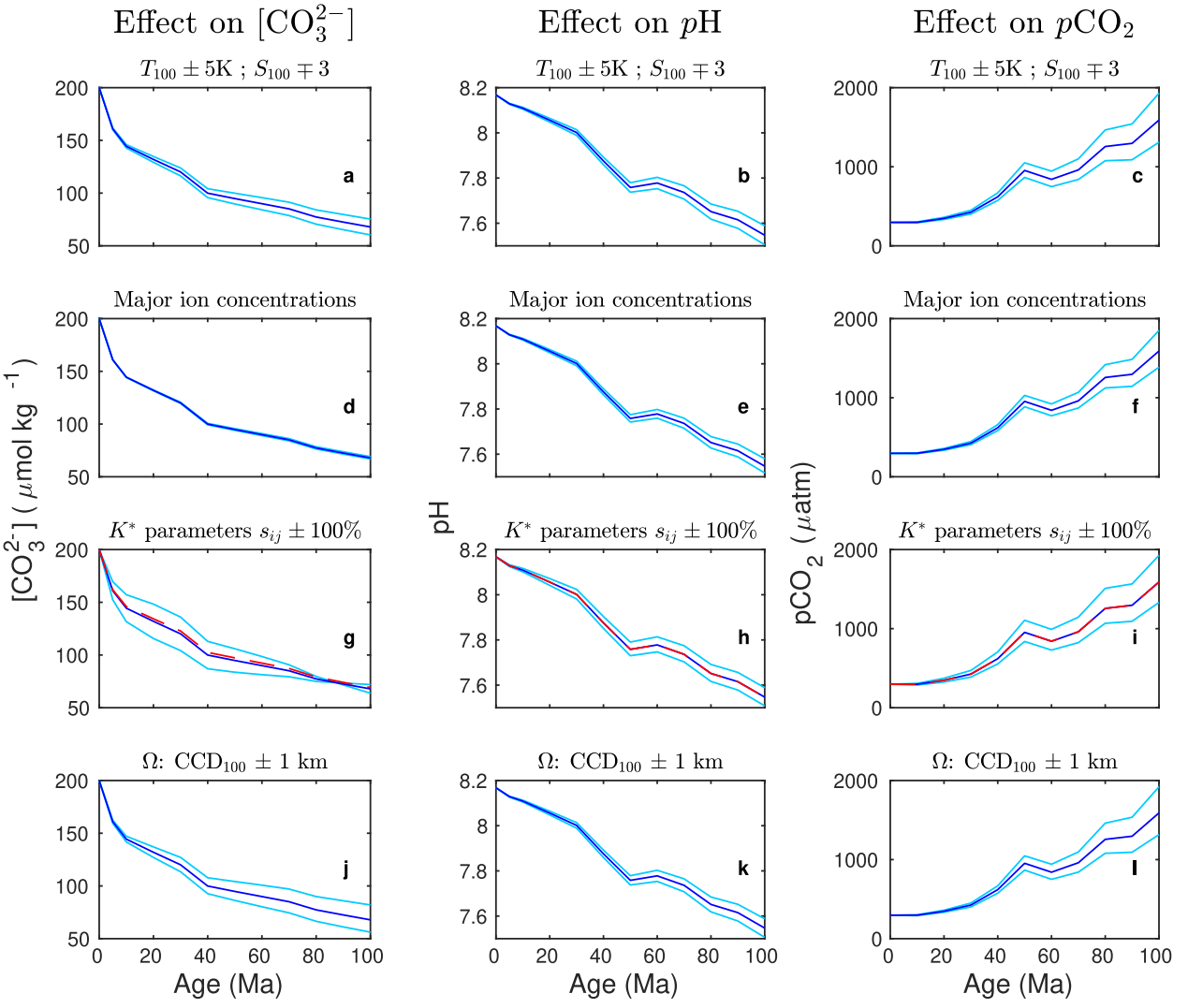

Fig. 8. Individual error propagation of critical parameters for $[CO_3^{2-}]$ (column 1), pH (column 2), and pCO_2 (column 3) reconstructions. Dark blue: standard scenarios, light blue: upper and lower uncertainty bounds for assigned parameter errors (see text for details). Red dashed line (3rd row): $\gamma^F_{CO_3^{2-}}$ in IPM changed from 0.2 (default) to 0.3 (cf. Section B.1). (For interpretation of the references to colour in this figure legend, the reader is referred to the web version of this article.)

would result in pCO_2 values $\sim$ 250 μatm too low at 100 Ma for the example shown (and $\sim$ 100 μatm too low at 50 Ma). Changing $\gamma^F_{CO_3^{2-}}$ from 0.2 (default) to 0.3 in the IPM has virtually no effect on the results (cf. Section B.1). Variations in Ω (via CCD) have a noticeable effect on $[CO_3^{2-}]$ and pCO_2 (ca. ±300 μatm at 100 Ma), although the assigned maximum CCD error of ±1 km at 100 Ma is probably quite large (Fig. 8, 4th row).

5.3.2. Errors from assumed $[Ca^{2+}] \times [SO_4^{2-}]$ value

The standard values for $[Ca^{2+}]$ and $[SO_4^{2-}]$ vs. time compiled in Fig. 1a were derived by the fluid inclusion studies assuming constant, modern $[Ca^{2+}] \times [SO_4^{2-}]$ in the past. Additional Ca^{2+} and SO_4^{2-} concentrations were provided by these studies for different values of $[Ca^{2+}] \times [SO_4^{2-}]$. For example, using 1.0, 0.5, and 1.5 times the modern $[Ca^{2+}] \times [SO_4^{2-}]$ value results in $[Ca^{2+}]$ and $[SO_4^{2-}]$ of 16^{+4}_{-5} and 19^{+4}_{-5} mmol kg^{-1}-H_2O in the Eocene at ~37 Ma (Horita et al., 2002) and 26^{+2}_{-6} and 14^{+2}_{-6} mmol kg^{-1}-H_2O in the Cretaceous at ~100 Ma (Timofeeff et al., 2006). These uncertainty ranges are similar to the assigned parameter errors for $[Ca^{2+}]$ and $[SO_4^{2-}]$ in our Monte Carlo simulations (±5 mmol kg^{-1}, see Table 3 below) and are hence covered by our Monte Carlo error propagation (Section 5.3.3). Such parameter errors affect the equilibrium constants via x_j's (Eq. (10)) but not the sensitivity parameters s_{ij}, which are derived taking into account charge balance via $[Na^+]$ adjustment (Table 2) or constant ionic strength (Appendix D) for each combination of the x_j's within their relevant ranges (Fig. C.1). Larger errors in $[Ca^{2+}]$ and $[SO_4^{2-}]$ do increase the uncertainties in the reconstructed Na^+ concentration and flux based on charge balance (Fig. 2). Finally, we note that the Mg/Ca ratio of seawater, $(Mg/Ca)_{sw}$, as derived by fluid inclusion studies based on modern $[Ca^{2+}] \times [SO_4^{2-}]$ is consistent with independent estimates of $(Mg/Ca)_{sw}$ (see Fig. 1b and discussion in Horita et al. (2002)). Alternatively, instead of constant $[Ca^{2+}] \times [SO_4^{2-}]$, perhaps one could assume that past changes in $[Ca^{2+}]$ were accompanied by equivalent changes in $[SO_4^{2-}]$ to maintain charge balance. However, this would lead to different $(Mg/Ca)_{sw}$ ratios in the past and leave changes in $[Mg^{2+}]$ essentially unbalanced (Fig. 1).

5.3.3. Monte Carlo error propagation

In this section, we follow standard practice and assume that all errors are random and normally distributed (Central Limit Theorem), but note that in reality systematic errors are also possible. The effect of the allocated errors on the uncertainty of the results was determined using a Monte Carlo approach in which the entire calculation procedure was executed 1,000 times with randomly different errors (Fig. 9, Table 3). The uncertainties of the results are reported as $\pm 2\sigma$ (twice the standard deviation of 1,000 results).

For $[Ca^{2+}]$, $[Mg^{2+}]$, and $[SO_4^{2-}]$ we added normally distributed errors to the data with standard deviation equal to half of the distance to the envelope (95% of values in a normal distribution are within $\pm 2\sigma$ of the mean). Errors in $[Ca^{2+}]$, $[Mg^{2+}]$, and $[SO_4^{2-}]$ were applied regardless of age (Table 3), after which an exponential function was fit to data + errors. This leads to larger variations in the fit function in the past because its value is fixed to the modern concentration at $t = 0$ Ma (Fig. 9). To account for possible changes in the surface-to-deep $[CO_3^{2-}]$ gradient in the past (actually ratio), we randomly varied the ratio f/f_m, with $[CO_3^{2-}]_s = f[CO_3^{2-}]_d$ and indices s, d, and m refer to surface, deep, and modern. For details and a comprehensive discussion of the surface-to-deep ratio, see Appendix of TZ04. As above, errors in CCD, temperature, salinity, and f/f_m were assumed to grow linearly with time in the past. Variations in major ion composition, temperature, and salinity then lead to variations in the stoichiometric equilibrium constants K^*, which depend on these parameters (Fig. 9). Finally, the propagated uncertainty in $[CO_3^{2-}]$ from the combined errors of all parameters can be calculated (Fig. 9). For example, at 100 Ma, $2\sigma \simeq 18$ μmol kg^{-1} and hence we estimate that $[CO_3^{2-}]$ was about 2.3 to 4-fold lower at 100 Ma ($\sim 68 \pm 18$ μmol kg^{-1} for a modern value of 200 μmol kg^{-1}).

5.3.4. Summary: error propagation

Despite relatively large assumed parameter errors, the propagated uncertainties in our results are moderate, suggesting that our reconstruction method is robust. However, the degree of accuracy to which our results reflect reality most critically depends on the reconstructed major ion composition of seawater, particularly $[Ca^{2+}]$, for which we have to rely on literature values (Fig. 1).

5.4. Paleo-*p*H scale

Proper *p*H scales commonly used for modern seawater are the total scale and the seawater scale, which include $[HSO_4^-]$ (Eq. (B.7)) and $[HSO_4^-] + [HF]$ in their ionic medium standard state, respectively (e.g., Hansson, 1973; Dickson, 1990; Millero, 1995; Zeebe and Wolf-Gladrow,

Table 3
Assigned parameter errors (2σ) for the Monte Carlo simulation.

$[Ca^{2+}]$[a] mmol kg^{-1}	$[Mg^{2+}]$[a] mmol kg^{-1}	$[SO_4^{2-}]$[a] mmol kg^{-1}	f/f_m [b] –	CCD[b] m	SST[b] °C	SSS[b] –
5	8	5	0.2	500	2.5	1.5

[a] Independent of age.
[b] Maximum error at 100 Ma.

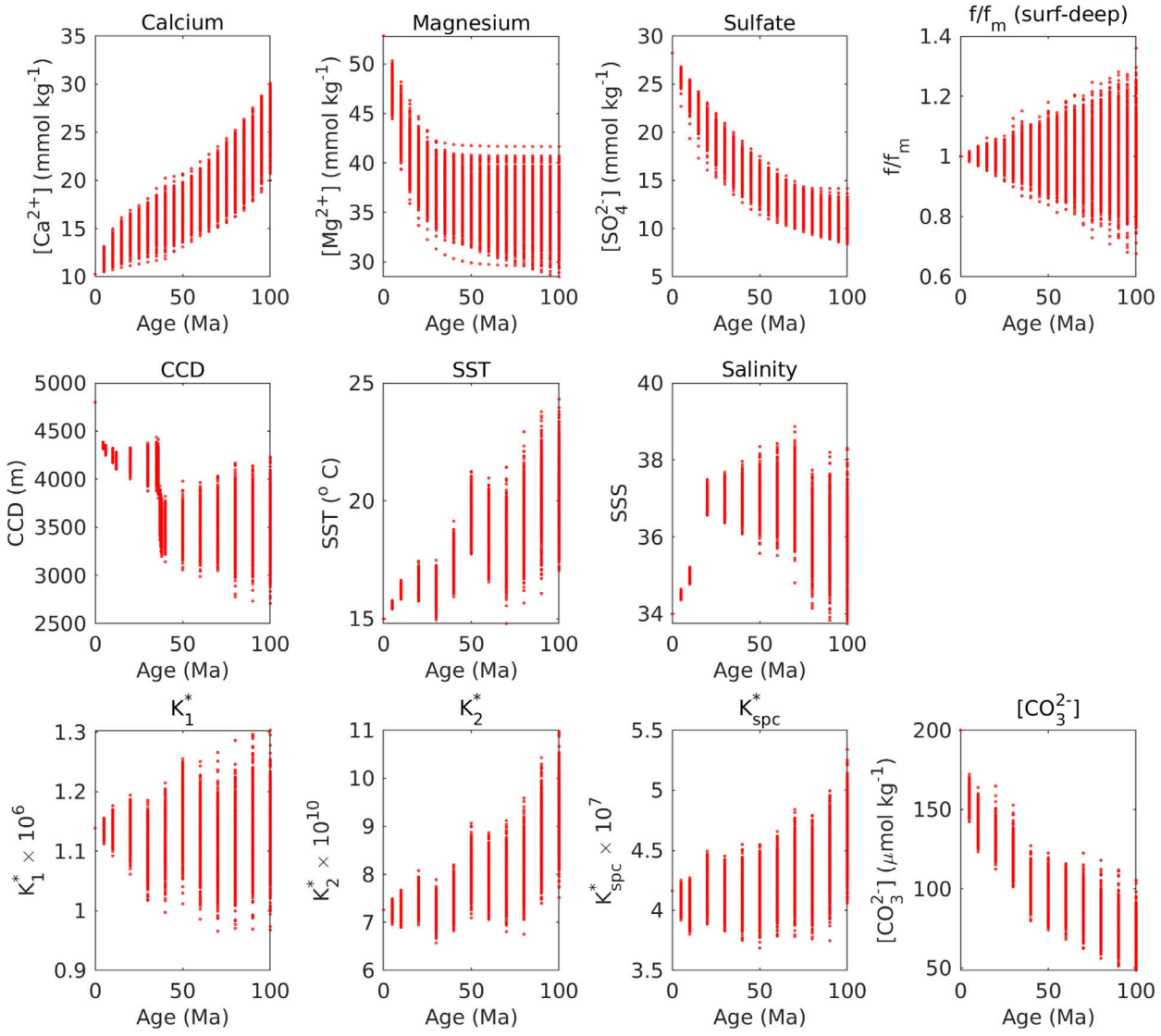

Fig. 9. Results of Monte Carlo simulation. Parameter variations were applied at 5–10 Myr time steps, see text. Each dot represents the result of a single run at that time step. Sea surface temperature (SST) after TZ04. Salinity from GEOCARB-III was used here for direct comparison with TZ04 but may be replaced by more recent estimates (the effect is small).

2001). We will focus here on the total scale as the concentration of fluoride in seawater is small and essentially unknown in the past. The fact that $[SO_4^{2-}]$ was lower in the past (Fig. 1a) represents a conceptual and practical problem when comparing paleo-*p*H and modern ocean *p*H. For instance, envision two hypothetical seawater samples of modern and, e.g., Paleocene age with otherwise identical composition but different sulfate concentrations, say modern and half of modern $[SO_4^{2-}]$. The two samples would give a different *p*H reading relative to a modern reference standard due to differences in $[SO_4^{2-}]$. The utility of the total *p*H scale in modern seawater implicitly relies on the constancy of the major components: "Sea water is an ionic medium [...] with practically constant composition of the major constituents" (Hansson, 1973); "The total concentrations of conservative constituents, such as borate, sulfate, and fluoride, can be estimated from salinity" (Dickson et al., 2007). None of the above, of course, holds for paleoseawater over time scales of millions of years. Hence labeling reconstructed *p*H values "pH_T" (e.g., derived from Cenozoic $\delta^{11}B$), where the subscript T refers to the modern concept of the total *p*H scale makes little sense in light of sulfate changes and should be avoided.

To illustrate the effect of $[SO_4^{2-}]$ on $[H^+]$, consider Eq. (B.7) and Fig. B.3. The ratio of free to total hydrogen ion concentration may be estimated from:

$$[H^+]_F/[H^+]_T \simeq 1/\left(1 + [SO_4^{2-}]/0.1\right). \quad (11)$$

For further illustration, assume $[H^+]_T$ to be constant. Then at half of modern $[SO_4^{2-}]$, Eq. (11) would give a ~12% higher free hydrogen ion concentration, or a ~0.05 units lower pH_F, relative to modern $[SO_4^{2-}]$. While this example is oversimplified compared to actual past seawater changes, it illustrates the effect of $[SO_4^{2-}]$ on pH, which, in turn affects speciation, including the $[B(OH)_3]/[B(OH)_4^-]$ fraction, a primary control on their $^{11}B/^{10}B$ ratio, which is critical for the pH proxy. As a result, changes in $[SO_4^{2-}]$ by themselves would affect pH reconstructions, even if all other conditions were the same. The bottom line is that the change in past $[SO_4^{2-}]$ (Fig. 1a) represents a conceptual and practical problem for determining paleo-seawater pH. The issue should be worked out properly for, e.g., $\delta^{11}B$-derived pH but is beyond the scope of this paper.

6. CONCLUSIONS

In this study, we have presented new reconstructions of past ocean carbonate chemistry and atmospheric CO_2 based on recent data and revised calculations. We also provide simple corrections for past equilibrium constants, supported by experimental data and well-suited for numerical models and observational studies on multi-million year time scales. Our updated result for just the seawater carbonate ion concentration (~2.3 to 4-fold lower 100 Myr ago) is similar to our earlier work (Tyrrell and Zeebe, 2004). This holds despite higher $[Ca^{2+}]$ from fluid inclusions >50 Ma (compared to TZ04), new chemistry routines, incorporation of $[SO_4^{2-}]$ effects, alternative CCD records, and extensive parameter variations, which suggests that our core approach is robust. However, all revised reconstructions using new alkenone and boron data now suggest similar to modern long-term ocean inventories of DIC and TA over the Cenozoic. This result contrasts with one of our earlier scenarios, which featured high Paleocene-Eocene DIC/TA inventories and was based on a now outdated boron record. Overall, our estimated long-term trends in CO_2 system parameters across the Cenozoic appear consistent, regardless of whether we combine our carbonate ion concentration with alkenone-derived pCO_2 or boron-derived pH. Our error analysis shows that despite relatively large assumed parameter errors, the propagated uncertainties in our results are moderate, lending confidence to our reconstruction method. However, the degree of accuracy to which our results reflect reality depends primarily on the fidelity of proxies for past major ion concentrations in seawater, particularly $[Ca^{2+}]$, which is independent of our work (Fig. 1). Finally, we have identified changes in past seawater sulfate as a conceptual and practical problem for determining paleo-seawater pH, which should be sorted out properly for the boron-pH proxy.

ELECTRONIC ANNEX

Our results displayed in Figs. 5,6 are electronically available at http://www.soest.hawaii.edu/oceanography/faculty/zeebe_files/ZT19.html.

ACKNOWLEDGMENTS

We thank Lee Kump and one anonymous reviewer for their constructive comments, which improved the paper. We are grateful to Dr. James William Buchanan Rae for sharing data compilations. Discussions with Gavin Foster, Sindia Sosdian, Yige Zhang, David Evans, Laura Haynes, and within the Research Coordination Network on Cenozoic pCO_2 (NSF OCE16-36005, Bärbel Hönisch) provided valuable details on proxy data. This research was supported by a NSF subaward of OCE13-38842 and NSF award OCE15-58699 to R.E.Z.

APPENDIX A. a_{H_2O} AND γ_{CO_2}

Changes in the activity of water (a_{H_2O}) and the activity coefficient of dissolved CO_2 (γ_{CO_2}) for solution compositions as reconstructed here are small. Moreover, for our approach only K^* ratios (past/modern) matter, hence the effect on the K_1^* ratio (see Eqs. (7) and (10)) is minor. The activity of water in seawater was estimated as a function of ionic strength, or salinity S (Millero and Leung, 1976; Lund et al., 2003):

$$a_{H_2O} = 1 - 5.0901 \times 10^{-4}\, S - 6.9567 \times 10^{-7}\, S^2. \quad (A.1)$$

For example, a salinity change from 35 to 33 (I from 0.72 to 0.68) would give a a_{H_2O} ratio of 1.001.

The CO_2 activity coefficient (γ_{CO_2}) for solutions of various seawater salts may described by:

$$\log \gamma_{CO_2} = k\, I, \quad (A.2)$$

where $k > 0$ (so-called salting out) depends on the type of salt. For the major seawater components, variations in k are moderate and have a minor effect on the ratio $\gamma_{CO_2}/\gamma^0_{CO_2}$ for $\gamma^0_{CO_2} = \gamma_{CO_2}(I = 0.7)$ (Fig. A.1). Hence we used Eq. (A.2) and adopted $k = 0.0946$ from the original IPM to calculate γ_{CO_2} (Millero and Schreiber, 1982).

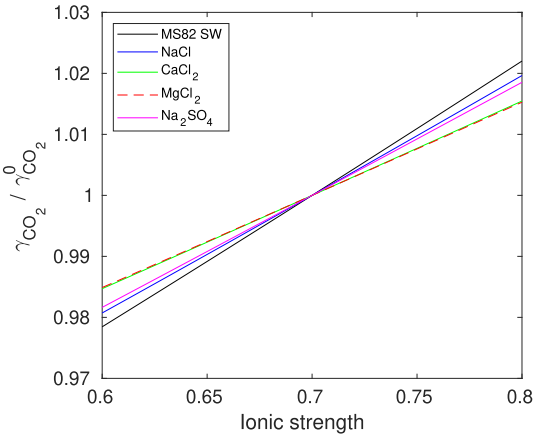

Fig. A.1. CO_2 activity coefficient ratio for $\gamma^0_{CO_2} = \gamma_{CO_2}(I = 0.7)$. Black line (MS82 SW): seawater (Millero and Schreiber, 1982). Parameters for other components are from He and Morse (1993).

APPENDIX B. $[Ca^{2+}]$, $[Mg^{2+}]$, $[SO_4^{2-}]$ EFFECTS ON K^*'S: DATA

B.1. $[Ca^{2+}]$

Calcium ions in seawater directly interact with major ions such as sulfate, as well as the dissolved carbonate species, including HCO_3^- and CO_3^{2-}. Hence changes in the seawater calcium concentration affect the activity of these ions and therefore the stoichiometric equilibrium constants. For example, with rising $[Ca^{2+}]$, the concentration of, e.g., $CaHCO_3^+$ rises, reducing $\gamma_{HCO_3^-}$. As a result, K_1^* should increase with $[Ca^{2+}]$ (see Eq. (7)). Importantly, this K_1^*-$[Ca^{2+}]$ relationship is confirmed by actual data (Fig. B.1) and is independent of any assumptions about activity coefficients (Eq. (7)), or the stability of $CaHCO_3^+$, or any other assumptions about ionic interactions.

Pytkowicz and Hawley (1974) and Rushdi and Chen-Tung (1995) (PH74 and RC95 for short) determined changes in apparent dissociation constants such as K_1' (Fig. B.1):

$$K_1' = \frac{a_H [HCO_3^-]}{[CO_2]}, \tag{B.3}$$

where a_H is the hydrogen ion activity defined in the NBS buffer scale (Mehrbach et al., 1973). Substituting activity coefficients as above and using $a_H = k\{H^+\}$, yields:

$$K_1' = K_1\, k\, \frac{\gamma_{CO_2}}{\gamma_{HCO_3^-}}\, a_{H_2O}, \tag{B.4}$$

where k is a correction resulting from pH measurements in concentrated solutions (Hawley and Pytkowicz, 1973). Eq. (B.4) is equivalent to PH74's Eq. (1) and shows that ratios of K_1', say at different $[Ca^{2+}]$, do not depend on γ_{H^+}, whereas ratios of K_1^* do (see Eq. (7)). If the solution is sulfate- and fluoride-free (as in PH74), γ_{H^+} should be essentially constant (see also Section B.3) and hence ratios of K_1' and K_1^* should be the same (cf. Eqs. (B.4) and (7)). However, RC95's artificial seawater (ASW) contained sulfate and fluoride (Kester et al., 1967). Thus, an increase in their ASW $[Ca^{2+}]$ would slightly lower free $[SO_4^{2-}]$ via Ca^{2+}-SO_4^{2-} interactions and hence increase free $[H^+]$ and γ_{H^+} (see Section B.3). As a result, the increase in K_1^* with $[Ca^{2+}]$ in ASW should be smaller than shown in Fig. B.1, which shows RC95's reported changes in apparent K_1'.

PH74 and RC95 experimentally determined K_1' and $K_1'K_2' = k^2 K_1 K_2 \gamma_{CO_2}/\gamma_{CO_3^{2-}}$, which both increase with $[Ca^{2+}]$ (Fig. B.1). The experimental trends are roughly captured by MS82's ion paring model (IPM, see note Section 3.1 though). However, with standard parameters, the IPM underestimates K_1' and overestimates absolute $K_1'K_2'$ values. This is not critical because our K^* corrections (see below) are based on trends, not absolute values. Nevertheless, one could attempt to reduce the data-model mismatch by changing model parameters such as the model's free activity coefficient of HCO_3^- ($\gamma^F_{HCO_3^-}$) in NaCl solutions from ~0.67 to ~0.65 and CO_3^{2-} ($\gamma^F_{CO_3^{2-}}$) from 0.2 to 0.3 (Fig. B.1). However, such changes in, e.g., $\gamma^F_{CO_3^{2-}}$ have virtually no effect on our final results (see Section 5.3).

While we do not recommend such parameter changes (for one, the IPM was designed for full seawater, not simplified solutions such as in PH74), one can ask if the $\gamma^F_{CO_3^{2-}}$ value of 0.3, for instance, would be within a range of values obtained from PH74's analysis. From PH74's data one may estimate $\gamma^F_{CO_3^{2-}}$ from $\gamma^F_{CO_3^{2-}} = k^2\, K_1\, K_2/K_1''K_2''$, where $k = 1.134$ and $K_1''K_2'' = 0.4866 \times 10^{-16}$ were both determined experimentally (Hawley and Pytkowicz, 1973; Hawley, 1973). Using values for K_1 and K_2 at 25 °C (Harned et al., 1941; Harned and Davis, 1943), gives $\gamma^F_{CO_3^{2-}} \simeq 0.55$ in NaCl solutions at $I = 0.72$. This is significantly higher than estimates for $\gamma^F_{CO_3^{2-}}$ in seawater at similar ionic strength and points to some inconsistency in PH74's data and/or analysis. One

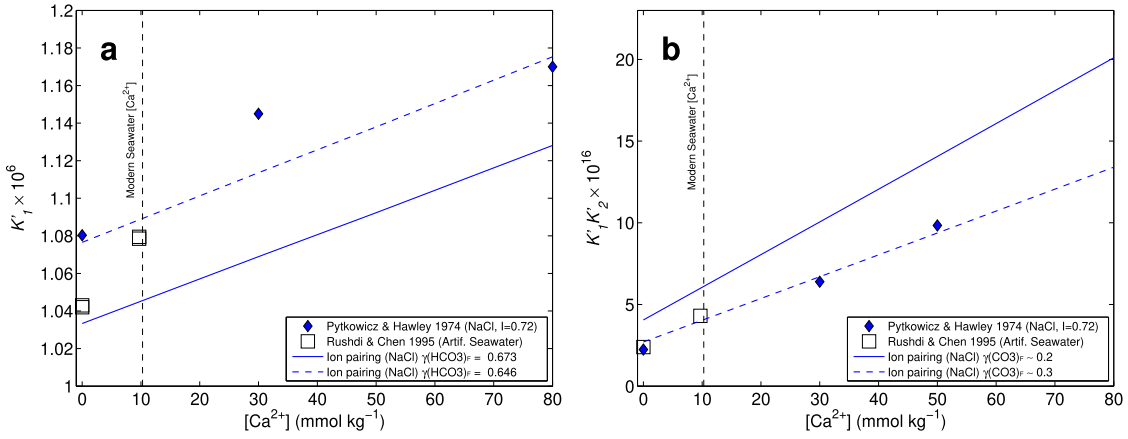

Fig. B.1. Measured (symbols) changes in (a) apparent K_1' and (b) $K_1'K_2'$ as a function of $[Ca^{2+}]$ in NaCl solutions and artificial seawater (ASW) both at constant ionic strength via adjusting [NaCl] at 25 °C (Pytkowicz and Hawley, 1974; Rushdi and Chen-Tung, 1995). Lines were calculated for PH74's NaCl solutions using their k, γ_{CO_2}, and a_{H_2O}, and an ion-pairing model based on Millero and Schreiber (1982). Note that changing $\gamma^F_{CO_3^{2-}}$ from 0.2 to 0.3 has virtually no effect on our final results (see Section 5.3).

possibility (speculation) is that PH74's analysis underestimated $K_1''K_2''$ and overestimated the stoichiometric association constant of $NaCO_3^-$ (Butler and Hutson, 1970; Millero and Schreiber, 1982; Millero and Thurmond, 1983). The above merely illustrates some of the uncertainties involved in both models and data of even seemingly simple NaCl-Ca^{2+}-HCO_3^- solutions. Note that seawater solutions are substantially more complex and that changing parameters to fit one particular data set may cause inconsistencies with another (e.g., for $\gamma_{CO_3^{2-}}$, see Section B.4).

B.2. $[Mg^{2+}]$

Similar to Ca^{2+}, Mg^{2+} interacts with various ions in seawater, including HCO_3^- and CO_3^{2-} and reduces their activity, which should increase stoichiometric (or apparent) constants with rising $[Mg^{2+}]$ (see Eqs. (7)–(9)). This behavior is confirmed by experimental studies in both NaCl solutions and ASW (Fig. B.2). The steeper slope indicated by Millero and Thurmond (1983)'s data (K^*'s) is likely due to the varying ionic strength of their Na-Mg-Cl solutions, which increased along with $[Mg^{2+}]$ ($I = [0.56\ 1.11]$). Again, the IPM (Millero and Schreiber, 1982) reproduces the values and trend for K_1' reasonably well but overestimates $K_1'K_2'$ (see discussion above). Importantly, the details of Mg-effects on dissociation constants for concentrations higher than modern ($[Mg^{2+}] > 53$ mmol kg^{-1}) are not critical for the present study because seawater $[Mg^{2+}]$ was likely lower than modern during much of the last 100 Myr (see Section 2).

Relevant data on K_1^* and K_2^* were also provided by He and Morse (1993). Unfortunately, measurements including changes in $[Ca^{2+}]$, $[Mg^{2+}]$, and $[SO_4^{2-}]$ were conducted at different I's and at 0, 50, 75, and 90 °C but not at 25 °C. In addition, possible interpolation to 25 °C is hindered by the fact that some of the data appear inconsistent. For example, the value for pK_1^* at $m_{SO_4^{2-}} = 1$ mmol kg^{-1} and 50 °C seems significantly too low compared to other temperatures (see their Table 2).

B.3. $[SO_4^{2-}]$

In seawater, SO_4^{2-} interacts with Mg^{2+}, Ca^{2+}, Na^+, etc. In addition, a significant fraction of hydrogen ion is bound to sulfate in the form of bisulfate ion:

$$HSO_4^- \rightleftharpoons H^+ + SO_4^{2-}, \tag{B.5}$$

with dissociation constant

$$K'_{HSO_4^-} = \frac{[H^+]_F [SO_4^{2-}]}{[HSO_4^-]}. \tag{B.6}$$

Note that $K'_{HSO_4^-}$ is given in terms of the free (not total) hydrogen ion concentration; hence the prime instead of an asterisk. Thus, changes in total seawater sulfate, $S_T = [SO_4^{2-}] + [HSO_4^-]$, cause changes in the free concentration of hydrogen ions. In fact, the bisulfate dissociation in seawater (Eq. (B.5)) represents the very basis for the total pH scale in seawater, where the total hydrogen ion concentration is given by (e.g., Hansson, 1973; Dickson, 1990):

$$[H^+]_T = [H^+]_F + [HSO_4^-] = [H^+]_F \left(1 + S_T / K'_{HSO_4^-}\right). \tag{B.7}$$

The effect of sulfate on, e.g., K_1^* and K_2^* may be illustrated by means of Eqs. (7) and (8). Assume for the moment that the activities of CO_2, HCO_3^-, and CO_3^{2-} remain constant. Then an increase in S_T would reduce $[H^+]_F$ (Eq. (B.5)) and hence γ_{H^+}. As a result, K_1^* and K_2^* would increase with the total sulfate concentration in seawater (Eqs. (7) and (8)). It turns out that changes in sulfate have a minor effect on the overall activities of CO_2, HCO_3^-, and CO_3^{2-},

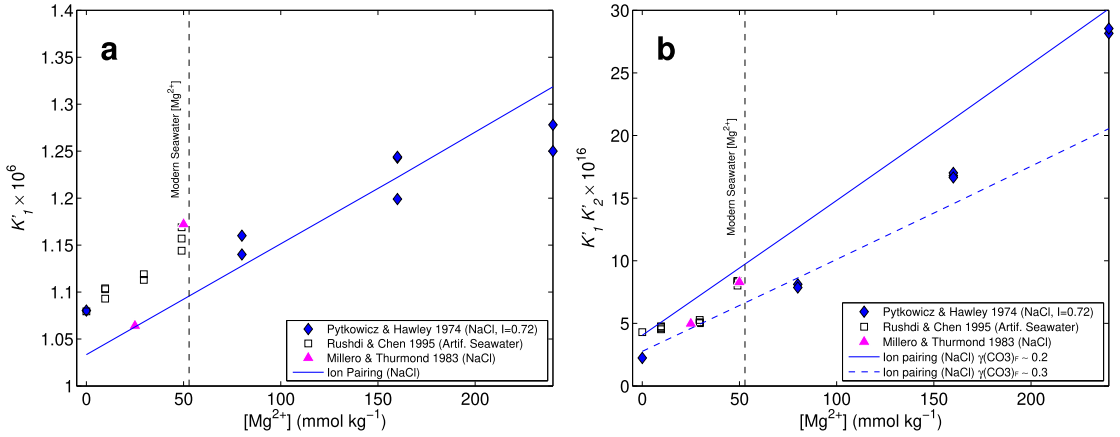

Fig. B.2. Measured (symbols) changes in (a) apparent K_1' and (b) $K_1'K_2'$ as a function of $[Mg^{2+}]$ in NaCl solutions and artificial seawater (ASW) both at constant ionic strength via adjusting [NaCl] at 25 °C (Pytkowicz and Hawley, 1974; Rushdi and Chen-Tung, 1995). The ionic strength of Millero and Thurmond (1983)'s Na-Mg-Cl solutions (triangles) increased along with $[Mg^{2+}]$, $I = [0.56\ 1.11]$ (higher I's not shown). Lines were calculated for PH74's NaCl solutions using an ion-pairing model based on Millero and Schreiber (1982). Note that Pytkowicz and Hawley (1974)'s and Rushdi and Chen-Tung (1995)'s data shown are for NaCl solutions without Ca^{2+} and ASW with Ca^{2+} (~9.7 mmol kg^{-1}), respectively. Note that changing $\gamma^F_{CO_3^{2-}}$ from 0.2 to 0.3 has virtually no effect on our final results (see Section 5.3).

which do not directly interact with SO_4^{2-} (though the direct effect on Ca^{2+} and hence calcite solubility is significant, see Fig. 3). Thus, given a value for $K'_{HSO_4^-}$, the effect of changing total seawater sulfate on K_1^* and K_2^* may be estimated.

Data for $K'_{HSO_4^-}$ have been obtained from galvanic cell measurements from which also the ratio $\gamma^T_{H^+}/\gamma^F_{H^+}$ as a function of S_T can be calculated (e.g., Khoo et al., 1977; Dickson, 1990) (Fig. B.3). For example, Khoo et al. (1977) determined HCl activity coefficients in ASW with and without sulfate. Rearranging their Eq. (3) yields an expression for the mean activity coefficient of HCl, $\gamma_\pm$(HCl), which can be evaluated using the data given in their Tables I and IV. The ratio $\gamma^T_{H^+}/\gamma^F_{H^+}$ at different S_T may then be estimated using the rule $\gamma_\pm = (\gamma_+\ \gamma_-)^{1/2}$ (Robinson and Stokes, 1959):

$$\gamma^T_{H^+}/\gamma^F_{H^+} = \gamma'^2_\pm(\mathrm{HCl})/\gamma^2_\pm(\mathrm{HCl}) \quad \text{(B.8)}$$

where primed and unprimed γ's refer to a given S_T and $S_T = 0$ (ASW with and without SO_4^{2-}), respectively. Note that SO_4^{2-} effects on γ_{Cl^-} should be small and hence γ_{Cl^-} and γ'_{Cl^-} cancel.

For Khoo et al. (1977)'s experimental conditions, Eq. (B.8) indicates a ~25% drop in $\gamma^T_{H^+}/\gamma^F_{H^+} = [H^+]_F/[H^+]_T$ as S_T rises from 0 mmol kg^{-1} to seawater values of ~28 mmol kg^{-1} (S_T scaled linearly with salinity S) (Fig. B.3). A similar trend is obtained for $[H^+]_F/[H^+]_T$ ratios estimated from Eq. (B.7) with a constant $K'_{HSO_4^-} = 0.1$ taken from Dickson (1990) (Fig. B.3). The latter graph is shown merely to visualize Eq. (B.7), which uses S_T and is plotted for constant $K'_{HSO_4^-}$. Eq. (B.7) is not supposed to fit Khoo et al. (1977)'s data which were obtained at low pH (requiring consideration of $[SO_4^{2-}]$ instead of S_T) and varying salinity/ionic strength (I). Rather, the data should fit the expression $[H^+]_F = [H^+]_T/\left(1 + [SO_4^{2-}]/K'_{HSO_4^-}\right)$, where $K'_{HSO_4^-}$ varies with I. Using $K'_{HSO_4^-}$ from Khoo et al. (1977), this is indeed the case (Fig. B.3) and is unsurprising because $K'_{HSO_4^-}$ was actually derived by a data fit of a similar kind (Khoo et al., 1977). In summary, the free hydrogen ion concentration decreases, and hence K_1^* and K_2^* increase, with the total sulfate concentration in seawater (Eqs. (7) and (8)).

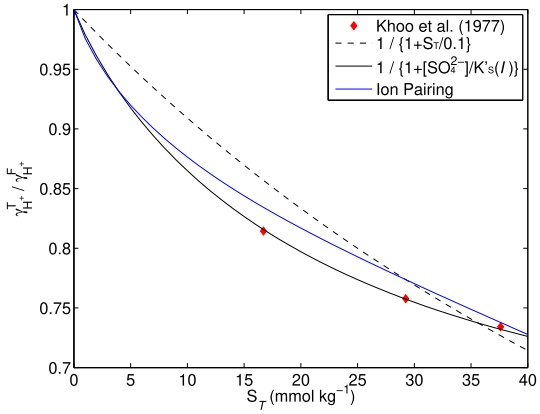

Fig. B.3. Effect of total sulfate on the ratio of hydrogen ion activity coefficients $\gamma^T_{H^+}/\gamma^F_{H^+} = [H^+]_F/[H^+]_T$ at 25 °C. Diamonds: based on Khoo et al. (1977)'s Eq. (3), data in their Tables I and IV ([HCl] = 0.01 mol kg^{-1}), and Eq. (B.8). Dashed black line: $[H^+]_F/[H^+]_T$ from Eq. (B.7) using S_T and a constant $K'_{HSO_4^-} = 0.1$ taken from Dickson (1990) ($T_c = 25$ °C, $S = 35$). Solid black line: $1/\left(1 + [SO_4^{2-}]/K'_{HSO_4^-}\right)$ using $[SO_4^{2-}]$ and Khoo et al. (1977)'s $K'_{HSO_4^-}$, including its variation with ionic strength I. Blue line: ion-pairing model (Millero and Schreiber, 1982) using Khoo et al. (1977)'s solution compositions, $K'_{HSO_4^-}$, and their effective (real) ionic strength. (For interpretation of the references to colour in this figure legend, the reader is referred to the web version of this article.)

The magnitude of the predicted change in K_1^* and K_2^* with sulfate depends on $K'_{HSO_4^-}$ in seawater, which is challenging to determine analytically. At $T_c = 25$ °C and $S = 35$, Dickson (1990)'s value is ~20% higher than that given by Khoo et al. (1977) (Fig. B.4). In his approach, Dickson included estimates of changes in γ_{H^+} with [HCl]; Khoo et al. (1977) did not. Furthermore, Dickson's values > 25 °C are in close agreement with values based on a recent re-evaluation of existing data for $K'_{HSO_4^-}$ (Waters and Millero, 2013; Waters et al., 2014). Hence, in this study we use $K'_{HSO_4^-} = 0.1$ at $T_c = 25$ °C and $S = 35$ (Dickson, 1990). Importantly, this implies a weaker association constant $\beta_{HSO_4^-} = 1/K'_{HSO_4^-}$ for HSO_4^- (see Eq. (B.6)) than suggested by Khoo et al. (1977).

B.4. Calcite solubility

It appears that few experimental studies have systematically examined the effect of $[Mg^{2+}]$ and $[Ca^{2+}]$ on the solubility product of calcite, K^*_{spc} (Eq. (6)). Mucci and Morse (1984) varied $[Mg^{2+}]$ in ASW up to about double the modern value at constant I (Fig. B.5). Calcium was kept close to modern values at ~10–12 mmol kg^{-1} except for one run with half of modern $[Ca^{2+}]$ (labeled 0.5×[Ca]). As expected from Mg^{2+}-CO_3^{2-} interactions and Eq. (9), K^*_{spc} increases

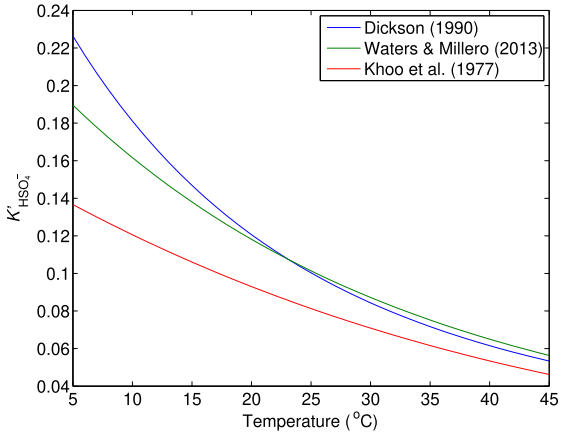

Fig. B.4. Values for $K'_{HSO_4^-}$, the dissociation constant of bisulfate in seawater as a function of temperature ($S = 35$) provided by different studies (Khoo et al., 1977; Dickson, 1990; Waters and Millero, 2013; Waters et al., 2014).

with $[Mg^{2+}]$. A comparable trend was found by Rushdi et al. (1998) in similar manipulations of ASW (Fig. B.5). The IPM (Millero and Schreiber, 1982) overestimates K^*_{spc} at higher $[Mg^{2+}]$ by ~10–20%. Note that if this mismatch was entirely attributed to model $\gamma_{CO_3^{2-}}$, then the inferred error would be much smaller than the inferred error in $\gamma_{CO_3^{2-}}$ based on $K'_1K'_2$ (discussed above).

Regarding uncertainties in the experimental results, it is important that both $[Ca^{2+}]$ and $[CO_3^{2-}]$ are required to determine K^*_{spc}. While Mucci and Morse (1984) measured $[Ca^{2+}]$ directly by titration, $[CO_3^{2-}]$ was derived from carbonate alkalinity, *p*H, and K'_2, where K'_2 was actually estimated based on ion pairing equations of Millero and Schreiber (1982). Rushdi et al. (1998) also involved K'_2 to calculate $[CO_3^{2-}]$ but it is not obvious from their description what values they used for K'_2. The K^*_{spc} values of those studies are thus not 'true' experimental values because they partly rely on theoretical estimates of K'_2 in ASW of varying compositions to derive $[CO_3^{2-}]$. Hence, in addition to measurement uncertainties, the K^*_{spc} values from experiments in ASW shown in Fig. B.5 are also subject to errors in K'_2 and $[CO_3^{2-}]$ estimates.

Additional calcite solubility studies are available in the literature, including He and Morse (1993) who stated that calcite solubility in three synthetic brines was measured and referred to $m_{CO_3^{2-}}$ as analytical data but no details were given and no values for K^*_{spc} and $m_{CO_3^{2-}}$ were listed. Gledhill and Morse (2006) reported calcite solubility in Na-Ca-Mg-Cl brines up to $I \simeq 4.5$. However, I varied substantially, the carbonate ion concentration was calculated using a Pitzer model, and most low-I data had very similar Mg^{2+} and Ca^{2+} concentrations, which is unhelpful for the current problem. Wolf et al. (1989) studied calcite solubility in different electrolytes, yet only Pitzer-calculated K^*_{spc} values were provided for NaCl solutions. We are not aware of a study that systematically varied $[Ca^{2+}]$ at constant ionic strength and provided measured values for K^*_{spc}. Note that Ca^{2+} directly affects K^*_{spc} through its activity coefficient (see Eq. (9)) and indirectly via interactions with CO_3^{2-}.

Mucci et al. (1989) provided a K^*_{spc} value for sulfate-free ASW (labeled 0×[SO4], Fig. B.5). However, experiments were only conducted at 25 °C and K'_2 was again estimated based on an ion pairing model. Several industrial/engineering studies are also available on calcite solubility in mixed electrolytes including SO_4^{2-} (e.g., Chong and Sheikholeslami, 2001; Shi et al., 2013; Dai et al., 2017). However, these studies calculated $[CO_3^{2-}]$ using thermodynamic constants or Pitzer equations, were restricted to 60–80 °C (Chong and Sheikholeslami, 2001), or to a single high NaCl background concentration >4 M (Shi et al., 2013; Dai et al., 2017).

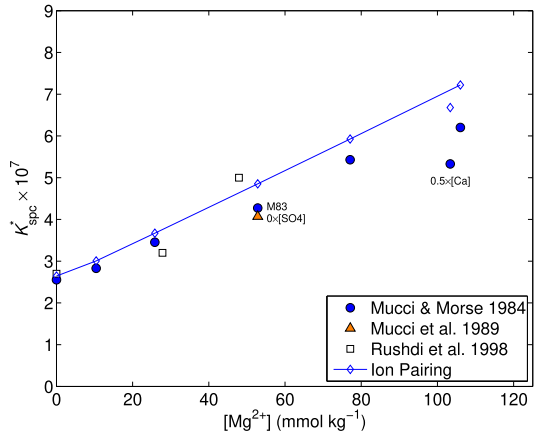

Fig. B.5. Changes in K^*_{spc} as a function of $[Mg^{2+}]$ from experiments in ASW at constant ionic strength via adjusting [NaCl] at 25 °C (symbols); M83 = Mucci (1983). Data points labeled 0.5×[Ca] and 0×[SO4] refer to ASW at half seawater-$[Ca^{2+}]$ and sulfate-free ASW (Mucci et al., 1989). The open diamonds were calculated for Mucci and Morse's (1984) ASW solutions using an ion-pairing model based on Millero and Schreiber (1982).

APPENDIX C. K^* RATIOS

The K^* ratios calculated with the IPM are very nearly linear as a function of $[Ca^{2+}]$, $[Mg^{2+}]$, and $[SO_4^{2-}]$ (x_j's), even when the x_j's are varied in combination (illustrated for K^*_1 in Fig. C.1). Hence over the relevant x_j range for reconstructions over the past 100 Myr (Section 2), the full IPM results and the linear approximation (Eq. (10)) are essentially indistinguishable (planes are nearly flat, Fig. C.1). Differences are only discernible at low $[SO_4^{2-}]$, where two separate planes are visible. The root mean square errors of the linear approach for K^*_1, K^*_2, and K^*_{spc} relative to the IPM results are about 0.5%, 2%, and 1%, much smaller than the accuracy required here. The largest error occurs for K^*_2 at low $[SO_4^{2-}]$ and both high $[Ca^{2+}]$ and $[Mg^{2+}]$ (not shown). However, this is of minor importance for the present study because $[Ca^{2+}]$ and $[Mg^{2+}]$ are inversely correlated over much of the past 100 Myr (Section 2).

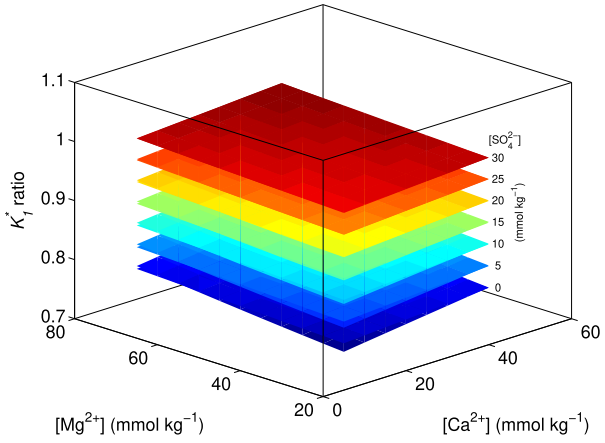

Fig. C.1. K^*_1 ratio (relative to modern) calculated with the IPM (Millero and Schreiber, 1982) and the linear approximation (Eq. (10)). The results are virtually indistinguishable, except at low $[SO_4^{2-}]$, where two separate planes are barely visible.

Table D.1
Sensitivity parameters $s_{ij} \times 10^3$ (dimensionless) for Eq. (10) at constant ionic strength via NaCl adjustment.

	K_1^*	K_2^*	K_{spc}^*
Ca^{2+}	6	156	171
Mg^{2+}	22	415	471
SO_4^{2-}	203	162	22

APPENDIX D. SENSITIVITY PARAMETERS FOR I = CONST.

See Table D.1.

APPENDIX E. CCD VARIATIONS AND Ω

Our surface $[CO_3^{2-}]$ is calculated from Eq. (1):

$$[CO_3^{2-}] = \Omega \cdot K_{sp}^*/[Ca^{2+}], \tag{E.9}$$

which includes the direct effect of past changes in $[Ca^{2+}]$, and T, S, $[Ca^{2+}]$, $[Mg^{2+}]$, and $[SO_4^{2-}]$ via K_{sp}^* on $[CO_3^{2-}]$. In addition, whole/deep-ocean saturation has varied somewhat in the past for which we apply a correction (β) based on CCD records (Tyrrell and Zeebe, 2004), i.e., $\Omega = \beta\, \Omega_m$ (m = modern). Note that Ω in the ocean at any z and at a given time t and $[Ca^{2+}]$ is a function of $[CO_3^{2-}]$ but not of $[Ca^{2+}]$ (homogeneous), because:

$$\Omega = \left([CO_3^{2-}]\ [Ca^{2+}]\right)/\left([CO_3^{2-}]_{sat}[Ca^{2+}]_{sat}\right) = [CO_3^{2-}]/[CO_3^{2-}]_{sat}. \tag{E.10}$$

The depth profile of the critical (saturation) $[CO_3^{2-}]_{sat}$, say modern, is given by:

$$c = a \exp[b(z - z_0)], \tag{E.11}$$

where a, b, z_0 are constants (Jansen et al., 2002). The crossover of *in situ* and saturation $[CO_3^{2-}]$ determines the depth of the saturation horizon z_{sh}. Specifically, consider Eq. (E.11) being applied twice, once for $c = c_{sh}$ at z_{sh} (at an initial $[CO_3^{2-}]$), and once for $c = c'_{sh}$ at a new z'_{sh} and a new $[CO_3^{2-}]$ (with $[Ca^{2+}]$ the same in both). Then c'_{sh}/c_{sh} provides a ratio relating changes in saturation to saturation depth (from Eq. (E.11)):

$$c'_{sh}/c_{sh} = \exp\left[b\left(z'_{sh} - z_{sh}\right)\right]. \tag{E.12}$$

For a given CCD (z_{cc}) at time t, the saturation horizon is $z_{sh} = z_{cc} - \Delta z$, hence:

$$c'_{sh}/c_{sh} = \exp\left[b\left(z'_{cc} - z_{cc}\right)\right], \tag{E.13}$$

assuming that Δz does not vary with $[CO_3^{2-}]$ (all else being equal). Importantly, it is immaterial here whether Δz has varied in the past because it cancels out. For past conditions (subscript p), we can write:

$$\left(c'_{sh}/c_{sh}\right)_p = \exp\left[b_p\left(z'_{cc} - z_{cc}\right)_p\right], \tag{E.14}$$

i.e., the same relationship, except for b_p, which, however, only varies slightly. Between modern and, say, Eocene conditions (including a 10 K temperature rise), b changes by only ~13%. Also, variations in b have a small effect on our results. Thus, we correct (scale) our surface Ω with the corresponding deep ratio based on the CCD record over time ($z_{cc}(t)$) by:

$$\beta = \exp\{b[z_{cc}(t) - z_{cc}(0)]\} \tag{E.15}$$

and quantify the sensitivity to changes in the surface-to-deep ratio by varying f/f_m (see Section 5.3.3 and Tyrrell and Zeebe (2004)).

REFERENCES

Anagnostou E., John E. H., Edgar K. M., Foster G. L., Ridgwell A., Inglis G. N., Pancost R. D., Lunt D. J. and Pearson P. N. (2016) Changing atmospheric CO_2 concentration was the primary driver of early Cenozoic climate. *Nature* **533**, 380–384.

Bartoli G., Hönisch B. and Zeebe R. E. (2011) Atmospheric CO_2 decline during the Pliocene intensification of Northern Hemisphere glaciations. *Paleoceanography* **26**, PA4213. https://doi.org/10.1029/2010PA002055.

Ben-Yaakov S. and Goldhaber M. B. (1973) The influence of sea water composition on the apparent constants of the carbonate system. *Deep-Sea Res.* **20**, 87–99.

Berner E. K. and Berner R. A. (2012). *Global Environment: Water, Air, and Geochemical Cycles*, second ed. Princeton University Press, Princeton, NJ.

Berner R. A. (2006) Inclusion of the weathering of volcanic rocks in the GEOCARBSULF model. *Am. J. Sci.* **306**, 295–302.

Berner R. A. (2008) Addendum to "Inclusion of the weathering of volcanic rocks in the GEOCARBSULF model": (R.A. Berner, 2006, V. 306, p. 295-302). *Am. J. Sci.* **308**, 100–103.

Berner R. A. and Kothavala Z. (2001) GEOCARB III: a revised model of atmospheric CO_2 over Phanerozoic time. *Am. J. Sci* **304**, 397–437.

Boudreau B. P. and Luo Y. (2017) Retrodiction of secular variations in deep-sea $CaCO_3$ burial during the Cenozoic. *Earth Planet. Sci. Lett.* **474**, 1–12.

Brennan S. T., Lowenstein T. K. and Cendon D. I. (2013) The major-ion composition of Cenozoic seawater: the past 36 million years from fluid inclusions in marine halite. *Am. J. Sci.* **313**, 713–775.

Butler J. N. and Huston R. (1970) Activity coefficients and ion pairs in the systems sodium chloride-sodium bicarbonate-water and sodium chloride-sodium carbonate-water. *J. Phys. Chem.* **74**(15), 2976–2983.

Caldeira K. and Berner R. (1999) Seawater ph and atmospheric carbon dioxide. *Science* **286**(5447), 2043a.

Chong T. H. and Sheikholeslami R. (2001) Thermodynamics and kinetics for mixed calcium carbonate and calcium sulfate precipitation. *Chem. Eng. Sci.* **56**(18), 5391–5400.

Coggon R. M., Teagle D. A. H., Smith-Duque C. E., Alt J. C. and Cooper M. J. (2010) Reconstructing past seawater Mg/Ca and Sr/Ca from mid-ocean ridge flank calcium carbonate veins. *Science* **327**, 1114.

Dai Z., Kan A. T., Shi W., Yan F., Zhang F., Bhandari N., Ruan G., Zhang Z., Liu Y., Alsaiari H. A., Lu Y.-T., Deng G. and Tomson M. B. (2017) Calcite and barite solubility measurements in mixed electrolyte solutions and development of a comprehensive model for water-mineral-gas equilibrium of the Na-K-Mg-Ca-Ba-Sr-Cl-SO_4-CO_3-HCO_3-CO_2(aq)-H_2O System up to 250 °C and 1500 bar. *Ind. Eng. Chem. Res.* **56**(23), 6548–6561.

Dickson A. G. (1990) Standard potential of the reaction: AgCl(s) + 1/2 H_2(g) = Ag(s) + HCl(aq), and and the standard acidity

constant of the ion HSO_4^- in synthetic sea water from 273.15 to 318.15 K. *J. Chem. Thermodyn.* **22**, 113–127.
Dickson A. G., Sabine C. L. and Christian J. R. (2007) Guide to Best Practices for Ocean CO_2 Measurements, vol. 3. PICES Special Publication, 191pp.
Dickson J. A. D. (2002) Fossil echinoderms as monitor of the Mg/Ca ratio of Phanerozoic oceans. *Science* **298**, 1222–1224.
Evans D. and Müller W. (2012) Deep time foraminifera Mg/Ca paleothermometry: nonlinear correction for secular change in seawater Mg/Ca. *Paleoceanography* **27**, PA4205.
Foster G. L., Lear C. H. and Rae J. W. B. (2012) The evolution of pCO_2, ice volume and climate during the middle Miocene. *Earth Planet. Sci. Lett.* **341**, 243–254.
Garrels R. M. and Thompson M. E. (1962) A chemical model for seawater at 25 °C and one atmosphere total pressure. *Am. J. Sci.* **260**, 57–66.
Gillis K. M. and Coogan L. A. (2011) Secular variation in carbon uptake into the ocean crust. *Earth Planet. Sci. Lett.* **302**, 385–392.
Gledhill D. K. and Morse J. W. (2006) Calcite solubility in Na-Ca-Mg-Cl brines. *Chem. Geol.* **233**, 249–256.
Gothmann A. M., Stolarski J., Adkins J. F., Schoene B., Dennis K. J., Schrag D. P., Mazur M. and Bender M. L. (2015) Fossil corals as an archive of secular variations in seawater chemistry since the Mesozoic. *Geochim. Cosmochim. Acta* **160**, 188–208.
Hansson I. (1973) A new set of pH-scales and standard buffers for sea water. *Deep-Sea Res.* **20**, 479–491.
Harned H. S. and Davis R. (1943) The ionization constant of carbonic acid in water and the solubility of carbon dioxide in water and aqueous salt solutions from 0 to 50 °C. *J. Am. Chem. Soc.* **65**(10), 2030–2037.
Harned H. S. and Scholes S. R. (1941) The ionization constant of HCO_3^- from 0 to 50 °C. *J. Am. Chem. Soc.* **63**(6), 1706–1709.
Hauzer H., Evans D., Müller W., Rosenthal Y. and Erez J. (2018) Calibration of Na partitioning in the calcitic foraminifer Operculina ammonoides under variable Ca concentration: toward reconstructing past seawater composition. *Earth Planet. Sci. Lett.* **497**, 80–91.
Hawley J. E. (1973) Bicarbonate and carbonate ion association with sodium, magnesium and calcium at 25 °C and 0.72 ionic strength. Ph. D. thesis, Oregon State University.
Hawley J. E. and Pytkowicz R. M. (1973) Interpretation of pH measurements in concentrated electrolyte solutions. *Mar. Chem.* **1**(3), 245–250.
Haynes L. L., Hönisch B., Dyez K. A., Holland K., Rosenthal Y., Fish C. R., Subhas A. V. and Rae J. W. B. (2017) Calibration of the B/Ca proxy in the planktic foraminifer Orbulina universa to Paleocene seawater conditions. *Paleoceanography* **32**, 580–599.
He S. and Morse J. W. (1993) The carbonic acid system and calcite solubility in aqueous Na-K-Ca-Mg-Cl-SO_4 solutions from 0 to 90 °C. *Geochim. Cosmochim. Acta* **57**, 3533–3554.
Hönisch B., Ridgwell A., Schmidt D. N., Thomas E., Gibbs S. J., Sluijs A., Zeebe R., Kump L., Martindale R. C., Greene S. E., Kiessling W., Ries J., Zachos J. C., Royer D. L., Barker S., Marchitto T. M., Moyer R., Pelejero C., Ziveri P., Foster G. L. and Williams B. (2012) The geological record of ocean acidification. *Science* **335**, 1058–1063.
Horita J., Zimmermann H. and Holland H. D. (2002) Chemical evolution of seawater during the Phanerozoic: implications from the record of marine evaporites. *Geochim. Cosmochim. Acta* **66**(21), 3733–3756.
Jansen H., Zeebe R. E. and Wolf-Gladrow D. A. (2002) Modeling the dissolution of settling $CaCO_3$ in the ocean. *Global Biogeochem. Cycles* **16**(2). https://doi.org/10.1029/2000GB001279.
Kester D. R., Duedall I. W., Connors D. N. and Pytkowicz R. M. (1967) Preparation of artificial seawater. *Limnol. Oceanogr.* **12**, 176–179.
Khoo K. H., Ramette R. W., Culberson C. H. and Bates R. G. (1977) Determination of hydrogen ion concentrations in seawater from 5 to 40 °C: standard potentials at salinities from 20 to 45 permil. *Anal. Chem.* **49**, 29–34.
Komar N., Zeebe R. E. and Dickens G. R. (2013) Understanding long-term carbon cycle trends: the late Paleocene through the early Eocene. *Paleoceanography* **28**, 650–662.
Kump L. R., Bralower T. J. and Ridgwell A. (2009) Ocean acidification in deep time. *Oceanography* **22**(4), 94–107.
Lécuyer C. (2016) Seawater residence times of some elements of geochemical interest and the salinity of the oceans. *Bull. Soc. géol. France* **187**(6), 245–260.
Lemarchand D., Gaillardet J., Lewin É. and Allègre C. J. (2002) Boron isotope systematics in large rivers: implications for the marine boron budget and paleo-pH reconstruction over the Cenozoic. *Chem. Geol.* **190**, 123–140.
Locklair R. E. and Lerman A. (2005) A model of Phanerozoic cycles of carbon and calcium in the global ocean: Evaluation and constraints on ocean chemistry and input fluxes. *Chem. Geol.* **217**, 113–126.
Lowenstein T. K. (2006) Elevated Eocene atmospheric CO_2 and its subsequent decline. *Science* **313**, 1928.
Lowenstein T. K., Hardie L. A. and Timofeeff M. N. (2003) Secular variation in seawater chemistry and the origin of calcium chloride basinal brines. *Geology* **31**, 857.
Lund M., Jönsson B. and Pedersen T. (2003) Activity coefficients in sea water using Monte Carlo simulations. *Mar. Chem.* **80**(2-3), 95–101.
Martínez-Botí M. A., Foster G. L., Chalk T. B., Rohling E. J., Sexton P. F., Lunt D. J., Pancost R. D., Badger M. P. S. and Schmidt D. N. (2015) Plio-Pleistocene climate sensitivity evaluated using high-resolution CO_2 records. *Nature* **518**, 49–54.
May P. M. and Rowland D. (2017) Thermodynamic modeling of aqueous electrolyte systems: current status. *J. Chem. Eng. Data* **62**(9), 2481–2495.
Mehrbach C., Culberson C. H., Hawley J. E. and Pytkowicz R. M. (1973) Measurement of the apparent dissociation constant of carbonic acid in seawater at atmospheric pressure. *Limnol. Oceanogr. 18*, 897–907.
Millero F. J. (1995) Thermodynamics of the carbon dioxide system in the oceans. *Geochim. Cosmochim. Acta* **59**, 661–677.
Millero F. J. and Leung W. H. (1976) The thermodynamics of seawater at one atmosphere. *Am. J. Sci.* **276**, 1035–1077.
Millero F. J. and Schreiber D. R. (1982) Use of the ion pairing model to estimate activity coefficients of the ionic components of natural waters. *Am. J. Sci.* **282**, 1508–1540.
Millero F. J. and Thurmond V. (1983) The ionization of carbonic acid in Na-Mg-Cl solutions at 25 °C. *J. Sol. Chem.* **12**(6), 401–412.
Montañez I. P. (2002) Biological skeletal carbonate records changes in major-ion chemistry of paleo-oceans. *Proc. Nat. Acad. Sci.* **99**, 15852–15854.
Mucci A. (1983) The solubility of calcite and aragonite in seawater at various salinities, temperatures, and one atmosphere total pressure. *Am. J. Sci.* **283**, 780–799.
Mucci A., Canuel R. and Zhong S. (1989) The solubility of calcite and aragonite in sulfate-free seawater and seeded growth kinetics and composition of precipitates at 25 °C. *Chem. Geol.* **74**, 309–329.
Mucci A. and Morse J. W. (1984) The solubility of calcite in seawater solutions of various magnesium concentration, I_t = 0.697 m at 25 °C and one atmosphere total pressure. *Geochim. Cosmochim. Acta* **48**, 815–822.
Pagani M., Huber M., Liu Z., Bohaty S. M., Henderiks J., Sijp W., Krishnan S. and DeConto R. M. (2011) The role of carbon dioxide during the onset of antarctic glaciation. *Science* **334**, 1261.

Pagani M., Zachos J. C., Freeman K. H., Tipple B. and Bohaty S. (2005) Marked decline in atmospheric carbon dioxide concentrations during the Paleogene. *Science* **309**, 600–603.

Pälike H., Lyle M. W., Nishi H., Raffi I., Ridgwell A., Gamage K., Klaus A., Acton G., Anderson L., Backman J., Baldauf J., Beltran C., Bohaty S. M., Bown P., Busch W., Channell J. E. T., Chun C. O. J., Delaney M., Dewangan P., Dunkley Jones T., Edgar K. M., Evans H., Fitch P., Foster G. L., Gussone N., Hasegawa H., Hathorne E. C., Hayashi H., Herrle J. O., Holbourn A., Hovan S., Hyeong K., Iijima K., Ito T., Kamikuri S.-I., Kimoto K., Kuroda J., Leon-Rodriguez L., Malinverno A., Moore, Jr., T. C., Murphy B. H., Murphy D. P., Nakamura H., Ogane K., Ohneiser C., Richter C., Robinson R., Rohling E. J., Romero O., Sawada K., Scher H., Schneider L., Sluijs A., Takata H., Tian J., Tsujimoto A., Wade B. S., Westerhold T., Wilkens R., Williams T., Wilson P. A., Yamamoto Y., Yamamoto S., Yamazaki T. and Zeebe R. E. (2012) A Cenozoic record of the equatorial Pacific carbonate compensation depth. *Nature* **488**, 609–614.

Pearson P. N., Foster G. L. and Wade B. S. (2009) Atmospheric carbon dioxide through the Eocene-Oligocene climate transition. *Nature* **461**, 1110–1113.

Pearson P. N. and Palmer M. R. (2000) Atmospheric carbon dioxide concentrations over the past 60 million years. *Nature* **406**, 695–699.

Pytkowicz R. M. and Hawley J. E. (1974) Bicarbonate and carbonate ion-pairs and a model of seawater at 25 °C. *Limnol. Oceanogr.* **19**(2), 223–234.

Rae J. W. B. (2018) Boron isotopes in foraminifera: systematics, biomineralisation, and CO_2 Reconstruction. In *Boron Isotopes* (eds. H. Marschall and G. Foster). Springer, pp. 107–143.

Ramette R. W. (2004) Gravimetric titrations: in support of weight titration techniques. *J. Chem. Educ.* **81**, 1715.

Rausch S., Böhm F., Bach W., Klügel A. and Eisenhauer A. (2013) Calcium carbonate veins in ocean crust record a threefold increase of seawater Mg/Ca in the past 30 million years. *Earth Planet. Sci. Lett.* **362**, 215–224.

Raven J. and Crawfurd K. (2012) Environmental controls on coccolithophore calcification. *Mar. Ecol. Progr. Ser.* **470**, 137–166.

Ridgwell A. and Schmidt D. (2010) Past constraints on the vulnerability of marine calcifiers to massive carbon dioxide release. *Nature Geosci.* **3**, 196–200. https://doi.org/10.1038/ngeo755.

Ries J. B. (2004) Effect of ambient Mg/Ca ratio on Mg fractionation in calcareous marine invertebrates: A record of the oceanic Mg/Ca ratio over the Phanerozoic. *Geology* **32**, 981.

Robinson R. A. and Stokes R. H. (1959) *Electrolyte solutions*, second ed. Butterworth's, London, p. 559.

Rohling E. J., Sluijs A., Dijkstra H., Köhler R. v. d. W. P., von der Heydt A., Beerling D., Berger A., Bijl P., Crucifix M., deConto R., Drijfhout S., Fedorov A., Foster G., Ganopolski A., Hansen J., Hönisch B., Hooghiemstra H., Huber M., Huybers P., Knutti R., Lea D., Lourens L., Lunt D., Masson-Demotte V., Medina-Elizalde M., Otto-Bliesner B., Pagani M., Pälike H., Renssen H., Royer D., Siddall M., Valdes P., Zachos J. and Zeebe R. (2012) Making sense of palaeoclimate sensitivity. *Nature* **491**, 683–691. https://doi.org/10.1038/nature11574.

Rushdi A. I. and Chen-Tung A. C. (1995) Variation of the apparent dissociation constants of carbonic acid with magnesium and calcium concentrations in seawater. *Atmos. Ocean. Sci.* **6**(2), 347–361.

Rushdi A. I., Chen-Tung A. C. and Suess E. (1998) The solubility of calcite in seawater solution of different magnesium concentrations at 25 °C and 1 atm total pressure: a laboratory re-examination. *La mer* **36**, 9–22.

Seki O., Foster G. L., Schmidt D. N., Mackensen A., Kawamura K. and Pancost R. D. (2010) Alkenone and boron-based Pliocene pCO_2 records. *Earth Planet. Sci. Lett.* **292**, 201–211.

Shi W., Kan A. T., Zhang N. and Tomson M. (2013) Dissolution of calcite at up to 250 °C and 1450 bar and the presence of mixed salts. *Ind. Eng. Chem. Res.* **52**(6), 2439–2448.

Sosdian S. M., Greenop R., Hain M. P., Foster G. L., Pearson P. N. and Lear C. H. (2018) Constraining the evolution of Neogene ocean carbonate chemistry using the boron isotope pH proxy. *Earth Planet. Sci. Lett.* **498**, 362–376.

Stanley S. M. and Hardie L. A. (1998) Secular oscillations in the carbonate mineralogy of reef-building and sediment-producing organisms driven by tectonically forced shifts in seawater chemistry. *Palaeogeogr., Palaeoclimatol., Palaeoecol.* **144**, 3–19.

Stefánsson A., Bénézeth P. and Schott J. (2013) Carbonic acid ionization and the stability of sodium bicarbonate and carbonate ion pairs to 200 °C - a potentiometric and spectrophotometric study. *Geochim. Cosmochim. Acta* **120**, 600–611.

Stefánsson A., Bénézeth P. and Schott J. (2014) Potentiometric and spectrophotometric study of the stability of magnesium carbonate and bicarbonate ion pairs to 150 °C and aqueous inorganic carbon speciation and magnesite solubility. *Geochim. Cosmochim. Acta* **138**, 21–31.

Stefánsson A., Lemke K. H., Bénézeth P. and Schott J. (2017) Magnesium bicarbonate and carbonate interactions in aqueous solutions: An infrared spectroscopic and quantum chemical study. *Geochim. Cosmochim. Acta* **198**, 271–284.

Sundquist E. T. (1986) Geologic Analogs: Their value and limitations in carbon dioxide research. In *The Changing Carbon cycle: A Global Analysis* (eds. J. R. Trabalka and D. E. Reichle). Springer-Verlag, New York, pp. 371–402.

Sundquist E. T. (1999) Seawater ph and atmospheric carbon dioxide. *Science* **286**(5447), 2043a.

Super J. R., Thomas E., Pagani M., Huber M., O'Brien C. and Hull P. M. (2018) North Atlantic temperature and pCO_2 coupling in the early-middle Miocene. *Geology* **46**, 519–522.

Timofeeff M. N., Lowenstein T. K., da Silva M. A. M. and Harris N. B. (2006) Secular variation in the major-ion chemistry of seawater: evidence from fluid inclusions in Cretaceous halites. *Geochim. Cosmochim. Acta* **70**, 1977–1994.

Tyrrell T. and Zeebe R. E. (2004) History of carbonate ion concentration over the last 100 million years. *Geochim. Cosmochim. Acta* **68**(17), 3521–3530.

Waters J., Millero F. J. and Woosley R. J. (2014) Corrigendum to The free proton concentration scale for seawater pH,, [MARCHE: 149 (2013) 8–22]. *Mar. Chem.* **165**, 66–67.

Waters J. F. and Millero F. J. (2013) The free proton concentration scale for seawater pH. *Mar. Chem.* **149**, 8–22.

Wolf M., Breitkopf O. and Puk R. (1989) Solubility of calcite in different electrolytes at temperatures between 10 ° and 60 °C and at CO_2 partial pressures of about 1 kPa. *Chem. Geol.* **76**, 291–301.

Zeebe R. E. (2012a) History of seawater carbonate chemistry, atmospheric CO_2, and ocean acidification. *Annu. Rev. Earth Planet. Sci* **40**, 141–165.

Zeebe R. E. (2012b) LOSCAR: long-term ocean-atmosphere-sediment carbon cycle reservoir model v20.4. *Geosci. Model Dev.* **5**, 149–166.

Zeebe R. E. and Tyrrell T. (2018) Comment on "The Effects of Secular Calcium and Magnesium Concentration Changes on the Thermodynamics of Seawater Acid/Base Chemistry: Implications for Eocene and Cretaceous Ocean Carbon Chemistry and Buffering"by Hain et al. (2015). *Global Biogeochem. Cycles* **32**. https://doi.org/10.1002/2017GB005786.

Zeebe R. E. and Wolf-Gladrow D. A. (2001) *CO_2 in Seawater: Equilibrium, Kinetics, Isotopes*. Elsevier Oceanography Series, Amsterdam, p. 346.

Zeebe R. E., Zachos J. C. and Dickens G. R. (2009) Carbon dioxide forcing alone insufficient to explain palaeocene-eocene thermal maximum warming. *Nature Geosci.* **2**, 576–580. https://doi.org/10.1038/ngeo578.

Zhang Y. G., Pagani M., Liu Z., Bohaty S. M. and DeConto R. (2013) A 40-million-year history of atmospheric CO_2. *Phil. Trans. Royal Soc. London A* **371**, 20130096.

Zhou X., Si W., Erez J., Rosenthal Y. (2018) Foraminiferal Na/Ca suggests decreased seawater Ca concentration and reduced hydrothermal activity since Mid-Miocene. In Goldschmidt Abstracts 2018.

Associate editor: Thomas M. Marchitto